Romanian Reports in Physics, Vol. 68, Supplement, P. S233–S274, 2016

COMBINED LASER GAMMA EXPERIMENTS AT ELI-NP

K. HOMMA[1,2], O. TESILEANU[3,*], L. D'ALESSI[3], T. HASEBE[1], A. ILDERTON[4], T. MORITAKA[5], Y. NAKAMIYA[6], K. SETO[3], H. UTSUNOMIYA[7], Y. XU[3]

[1]Graduate School of Science, Hiroshima University, Higashihiroshima, Hiroshima, Japan

[2]International Center for Zetta-Exawatt Science and Technology, École Polytechnique

[3]ELI-NP, "Horia Hulubei" National Institute for Physics and Nuclear Engineering, 30 Reactorului Street, RO-077125, Bucharest-Magurele, Romania

[4]Department of Applied Physics, Chalmers University of Technology, Maskingrand 2, 412 58 Gothenberg, SE-41296, Sweden

[5]Department of Physics, National Central University, No.300, Jhongda Rd., Jhongli District, Taoyuan city 32001, Taiwan

[6]Institute of Chemical Research, Kyoto University, Gokasho, Uji-city, Kyoto, 611-001, Japan

[7]Department of Physics, Konan University, 8-9-1, Okamoto, Higashi-nada, Kobe, Hyogo, 658-8501, Japan

[*]Corresponding author *E-mail:* ovidiu.tesileanu@eli-np.ro

Abstract. We propose experiments in the E7 and E4 experimental areas at ELI-NP to tackle problems of fundamental physics, taking advantage of the unique configuration and characteristics of the new research infrastructure to be constructed in Magurele, Romania. The experimental setups proposed follow a gradual approach from the point of view of complexity, from the "Day 1" experiments to experiments for which the prerequisites include results from the previously performed ones. In addition, there are two generic Research and Development tasks proposed in this Technical Design Report (TDR), related to the development of a detection system, Gamma Polari-Calorimeter (GPC), commonly applicable to energy measurements for electrons, positrons and gamma-rays above the 0.1 GeV energy scale and the preparatory tests for laser plasma acceleration of electrons up to necessary energies 210 MeV, 2.5 GeV and 5 GeV for the later stage experiments, respectively. In this paper we particularly focus on possible "Day-1" topics and briefly mention the future extensions foreseen.

Key words: High-intensity laser, LINAC based gamma-ray source, isomers, photoexcitation, dark matter survey, 4-wave mixing, gamma polari-calorimeter, non-linear QED, radiation reaction, pair production, gamma-gamma collider, vacuum birefringence

1. INTRODUCTION

This TDR is the result of the collaboration between the authors and the ELI-NP employees and scientists from universities and research institutes from Japan and Korea.

The contributors from ELI-NP, in alphabetical order are: Sohichiroh Aogaki, Bertrand Boisdeffre, Mihail Cernaianu, Ioan Dancus, Dan Filipescu, Cristian Petcu, Mihai Risca and Zafar Yasin.

The external contributors are: Yasuo Arai (KEK, Japan), Masaki Hashida (Kyoto University, Japan), Yoshihisa Iwashita (Kyoto University, Japan), Masaki Kando (JAEA, Japan), James Koga (JAEA, Japan), Tetsuro Kumita (Tokyo Metropolitan University), Kayo Matsuura (Hiroshima University, Japan), Kazuhisa Nakajima (Institute for Basic Science, Korea), Shuji Sakabe (Kyoto University, Japan).

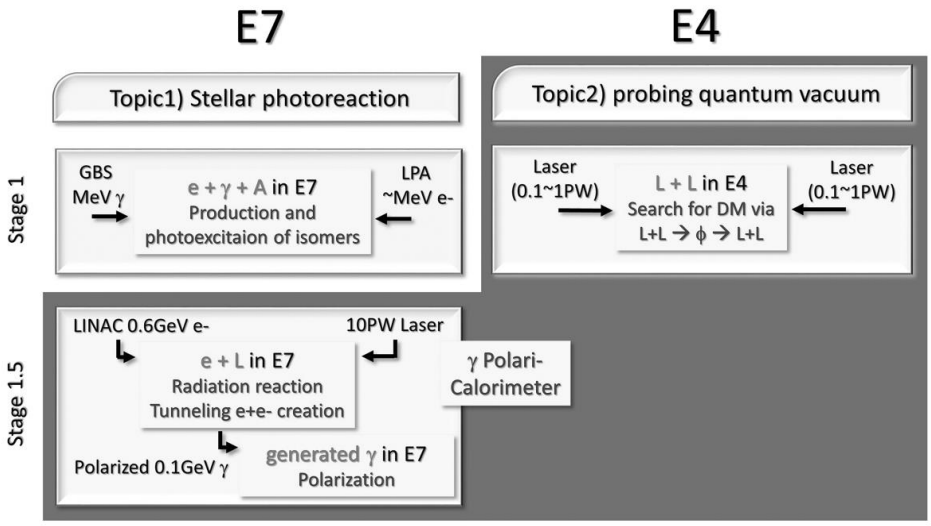

Figure 1 - The Physics cases in RA5-TDR (early half plan).

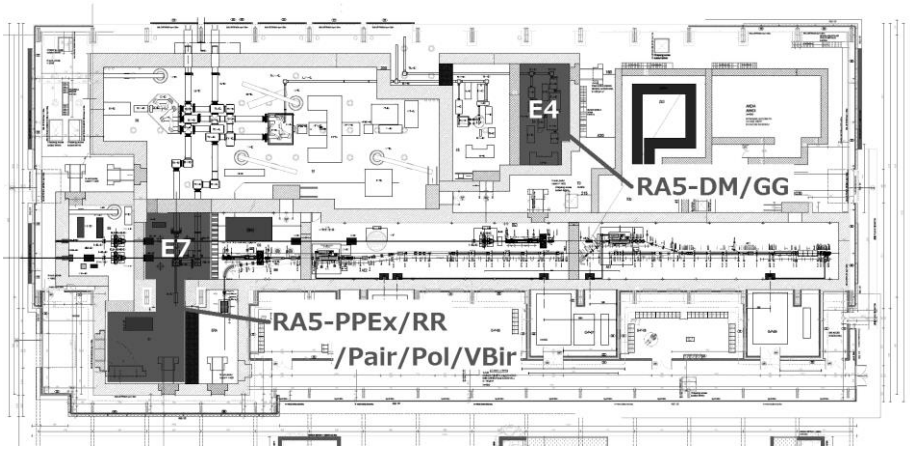

Figure 2 - The work space for the proposals in RA5-TDR.

This proposal includes two main topics in physics with staged developments to gradually tackle them. The first is nuclear reactions, linked to the possibility to reach, at ELI-NP, conditions encountered in the interior of stars – the production and photoexcitation of isomers is proposed. The second topic is probing the photon-photon interactions below the MeV energy scale in general which have not been explored thoroughly to date by utilizing the laser-laser, laser-gamma and gamma-gamma collision systems. By these various combinations of photon beams, we can test sub-eV Dark Matter scenarios as well as nonlinear Quantum Electrodynamics (QED) effects both in perturbative and non-perturbative regimes. It also includes the laser-electron scattering for the fundamental tests on the radiation mechanisms and pair production via the tunneling process in extremely high-intensity laser fields. The laser-electron experiment also aims at the generation of polarized gamma-rays from sub-GeV to GeV as probes for the later stage experiments to explore the vacuum birefringence under high-intensity laser fields. Considering all of the above, we define several sections for the experiments performed at E7 and E4 experimental areas (Figure 1 and Figure 28 in Chapter 4).

We define experimental stages and the flow charts depending on the experimental areas, Research and Development subjects, and combinations of beam sources necessary for individual experimental proposals is shown in Figure 1, where abbreviations L, e, γ and A correspond to laser, electron, gamma-ray beams and nucleus targets, respectively.

“Stage 1” experiments correspond to technically less difficult proposals based on available beam sources within the current ELI-NP design.

At E7 the production of isomers by using MeV electrons produced with one 1 PW/10 PW laser line and the excitation with gamma radiations from the Gamma

Beam System (GBS) will be measured via the observation of neutron emission. There are two irradiation modes in the production and photoexcitation of isomers: synchronized and non-synchronized irradiations of laser photons and gamma photons. These experiments are referred as "Production and Photoexcitation of isomers experiments" or RA5-PPEx.

At E4 the search for weakly coupling sub-eV Dark Matter (RA5-DM) with two 0.1 PW lasers and then two 1 PW lasers, will be performed. This is the simplest experiment that utilizes only the laser beams in vacuum chambers.

The prime Research and Development topic necessary for the following stages 1.5, 3 and 4 is the development of the common detector, Gamma Polari-Calorimeter (GPC), to measure momenta of e^+ and e^-, energies of gamma-rays above 0.1 GeV and the degree of linear polarization of gamma-rays via the conversion process to e^+e^-. We refer to this Research and Development topic as RA5-GPC.

The second Research and Development subject is the generation of 210 MeV, 2.5 GeV and 5.0 GeV electron beams based on Laser Plasma Acceleration (LPA) with gas cells for experimental proposals for the future upgrades.

Though we will perform proof-of-principle experiments at existing infrastructures prior to the operational phase of ELI-NP, we do not include specific proposals for this subject in our TDR, because other ELI-NP TDR teams also plan this kind of experiments and we will share the relevant technical information by the time of commissioning in 2018.

"Stage 1.5" proposals are fundamental tests on radiation reaction (RA5-RR), on pair production (RA5-Pair) and on degrees of linear polarization (RA5-Pol) via the extremely non-linear process in extremely high-intensity laser fields by combining 600 MeV electrons from the LINAC (ELI-NP Gamma Beam System) and a 10 PW laser at E7. All proposed measurements are possible with the GPC.

These experiments can be an alternative proposal to the E7 stage-1 experiment (RA5-PPEx) which shares the common interaction chamber at E7. Depending on the advances of the preparatory experiments relevant to RA5-PPEx and on the decision to construct the electron transport line to E7, the staging order between L(e) + γ + A (RA5-PPEx) and e (0.6 GeV) + L (RA5-RR, -Pair, -Pol) may be swapped. The stage 1.5 proposals require an additional electron transport line to the E7 area in order to get the accurately controlled stable electron bunches from the LINAC (of the Gamma Beam System). Also an additional Compton-scattering-based calibration system to synchronize one electron bunch with a 10 PW laser pulse must be in place. The electron bunches will arrive to E7 from the LINAC with a lower repetition rate of 1 Hz instead of 100 Hz, to reduce the electron current for the beam dump in E7. Therefore, it is foreseen to guide 1 PW laser pulses operated at 1 Hz into the E7 area (through the existing 10 PW beamlines) which is synchronized with 10 PW with a fixed time difference in advance. However, these additional implementations do not pose difficulties from the technical point of view.

Based on the following basic parameters for 0.1 PW, 1 PW and 10 PW lasers and for electrons from GBS LINAC, we briefly introduce in the following sub-sections the physics cases listed above.

Table 1
Parameters of the available laser output.

Power	0.1 PW	1 PW	10 PW
Pulse energy	2.2 J	22 J	220 J
Pulse duration	22 fs	22 fs	22 fs
Wave length	820 nm	820 nm	820 nm

Table 2
Parameters of the electron beam from GBS LINAC as used in the proposals.

Parameter	Value
Energy	600MeV
Bunch charge	4.5-100pC
Number of electrons (avg)	10^9
Energy spread FWHM	0.1%
Spot size	15 μm
Bunch length	100
Rep. rate of M27 kicking	1 Hz
Divergence	0.5 mm mrad

2. STAGE 1

2.1. Production and Photoexcitation of Isomers (RA5-PPEX)

2.1.1. Physics case

In nuclear astrophysics [1, 2], the reaction rate ($\lambda_{\gamma n}$), that is the number of reactions taking place per unit time, for a photoreaction induced on a ground-state nucleus leading to the emission of a neutron is given by

$$\lambda_{\gamma n} = \int_0^\infty c n_\gamma(E) \sigma_{\gamma n}(E) dE \,, \tag{2.1.1}$$

where c is the speed of light, $\sigma_{\gamma n}$ the photoneutron cross sections, and $n_\gamma(E)$ the number of photons per unit volume at energy E. In a stellar interior at a temperature T, $n_\gamma(E)$ is remarkably close to a black-body or Planck distribution:

$$n_\gamma(E,T)dE = \frac{1}{\pi^2}\frac{1}{(\hbar c)^3}\frac{E^2}{\exp(E/kT)-1}dE \,. \tag{2.1.2}$$

When Eq. (2.1.2) is substituted for $n_\gamma(E)$ in Eq. (2.1.1), the rate becomes a function of parameter T. It is then possible to define the photon energy range which is the most relevant for determining $\lambda_{\gamma n}(T)$ at the temperature of astrophysical interest. This results from the properties of the integrand of Eq. (2.1.1), the product of the photoneutron cross section $\sigma_{\gamma n}(E)$ and the Planck distribution $n_\gamma(E)$. The integrand differs significantly from zero only in a relatively small energy range defined immediately above neutron threshold. We call this range the Gamow window for photoneutron reactions. Figure 3 illustrates this Gamow window.

In stellar environments, nuclear excited states are thermally populated. Figure 4 depicts photoexcitation on a thermally populated excited state. At high temperatures, thermalization may enhance the photoreaction rates by several orders of magnitudes.

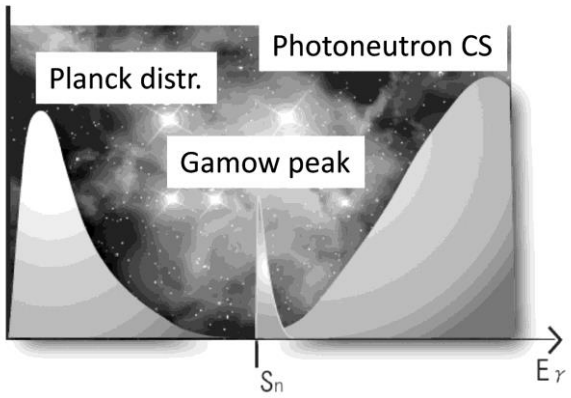

Figure 3 - The Gamow window for photoneutron reactions defined immediately above neutron threshold S_n. A narrow energy window is defined as the product of the photoneutron cross section and the Planck distribution.

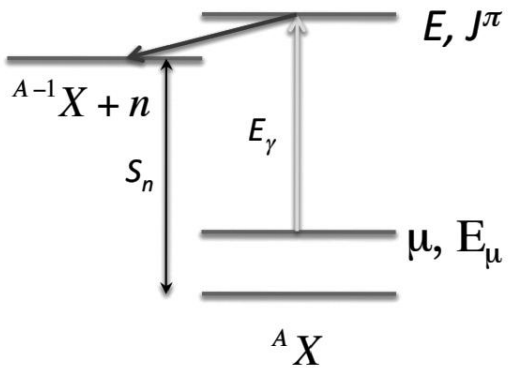

Figure 4 - Photoexcitation on the excited state.

The right-hand side of Eq. (2.1.1), which corresponds to photodisintegration from the ground state only, must be replaced by a sum of the rates $\lambda_{\gamma n}^{\mu}(T)$ for photodisintegration from all (ground and excited) states μ, each term being weighted by the appropriate Boltzmann factor. Thus, the astrophysical reaction rate λ^{*} is defined by

$$\lambda_{\gamma n}^{*}(T) = \frac{1}{G(T)} \sum_{\mu} \frac{2J^{\mu}+1}{2J^{0}+1} \lambda_{\gamma n}^{\mu}(T) \exp(-\varepsilon^{\mu} / kT) \tag{2.1.3}$$

where

$$G(T) = \sum_{\mu} \frac{2J^{\mu}+1}{2J^{0}+1} \exp(-\varepsilon^{\mu} / kT) \tag{2.1.4}$$

is the temperature-dependent partition function of the target nucleus. Note that in $\lambda_{\gamma n}^{\mu}(T)$, $\sigma_{\gamma n}(E)$ is replaced by the cross section $\sigma_{\gamma n}^{\mu}(E)$ for photodisintegration from state μ. Photoexcitation strength function $f_{XL}^{\mu}(E)^{\uparrow}$ is determined by the photoabsorption cross section $\sigma_{XL}^{\mu}(E)$ summed over all possible spins of the final states [3]:

$$f_{XL}^{\mu}(E)^{\uparrow} = \frac{E^{-2L+1}}{(\pi\hbar c)^{2}} \frac{\sigma_{XL}^{\mu}(E)}{2L+1} \tag{2.1.5}$$

Here, *X* represents the electric (*E*) or magnetic (*M*) excitation mode and *L* the multipolarity.

Although nuclear reactions naturally take place not only on the ground state but also on excited states thermally populated in the interior of stars, closed nuclear systems at high temperatures and densities formed by the gravitational force, they are induced only on the ground state in experimental laboratories on Earth. As a result, there is no experimental information on $\sigma_{\gamma n}^{\mu}(E)$, $\sigma_{XL}^{\mu}(E)$, and $f_{XL}^{\mu}(E)^{\uparrow}$ for

any excited state μ. Note that $\sigma_{\gamma n}^{\mu}(E) = \Sigma_{XL} T_{XL,n} / T_{XL}^{total} \times \sigma_{XL}^{\mu}(E)$, where $T_{XL,n}$ is the neutron transmission coefficient and T_{XL}^{total} the sum of all particle and radiative transmission coefficients. Above neutron threshold ($E > S_{n:}$ neutron separation energy), T_{XL}^{total} is generally dominated by $T_{XL,n}$ which becomes zero at S_n. Due to a lack of the experimental information, the Hauser-Feshbach statistical model is used to calculate $\sigma_{XL}^{\mu}(E)$, $T_{XL,n}$, T_{XL}^{total}, and $\sigma_{\gamma n}^{\mu}(E)$, assuming that the gamma-ray strength function $f_{XL}^{\mu}(E)$ is the same as the one for the ground state (Brink hypothesis [4]). Thus, it is indispensable to experimentally investigate stellar photoreactions in the laboratory.

The ELI-NP may become the first research laboratory where stellar photoreactions are induced and detected. We propose an experiment to induce stellar photoreactions at E7 by producing isomers with the high power lasers and photo-exciting isomers with the intense gamma-ray beam.

The experiments of producing the isomers may be performed either by multiple laser shots (Type I) or a single laser shot (Type II) of the 10 PW lasers. An isomer is produced in the inelastic electron scattering or in a photoabsorption reaction, leaving a nucleus in either bound states or unbound states; the bound states decay to the isomeric state via γ-transition [5], while the unbound states undergo neutron emission followed by γ-transition to the isomeric state [6]. Laser-accelerated electrons with kinetic energies of the order of MeV followed by the subsequent production of Bremsstrahlung radiation most effectively produce isomers. Therefore, a key technology is to produce a vast number of MeV electrons by laser acceleration suited to the production of isomers, by optimizing the operation condition of the laser with the pulse width of femtosecond.

The Type I experiment is applicable to long-lived isomers with half-lives sufficiently longer than the frequency (1/60 Hz) of the 10 PW laser. The production of a large number of long-lived isomers is required in the first step followed by subsequent irradiations with a gamma-ray beam in the second step to photo-excite the isomers. In contrast, the Type II experiment is applicable to all isomers irrespective of their half-lives because isomers are produced by a single laser shot and simultaneously irradiated with a gamma-ray beam that is synchronized to the laser shot. Since the laser shot and the gamma-ray irradiation are synchronized in a time interval of the order of ps, the Type II experiment is also applicable to excited state with half-lives comparable to the synchronization time. The signal-to-noise ratio, limited by the fact that a relatively small number of isomers are produced by a single laser shot is greatly improved by applying a short time gate for the synchronized irradiation of laser and gamma-ray beams. A Type II experiment for an isomer $^{155}Gd^{m}$ with a half-life of 32 ms is depicted in Figure 5. Table 3 lists isomers of research interest.

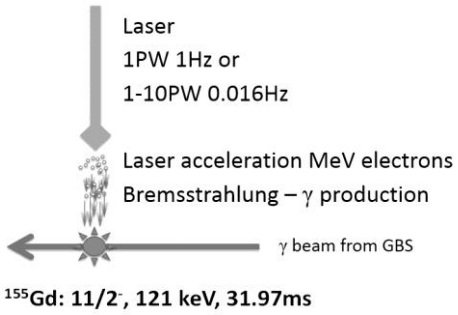

Figure 5 - Schematic image of the 4π neutron detector structure, proposed in the ELI-NP TDR "Gamma Above Neutron Threshold".

Table 3
Isomers of research interest

Isomers	J^{π}	E_x	Half-life
$^{189}Os^{m}$	$9/2^{-}$	30.8 keV	5.81 h
$^{180}Ta^{m}$	9^{-}	75.3 keV	> 1.2 x 10^{15} y
$^{176}Lu^{m}$	1^{-}	123 keV	3.66 h
$^{155}Gd^{m}$	$11/2^{-}$	121 keV	31.97 ms
$^{152}Eu^{m}$	0^{-}	45.6 keV	9.27 y
$^{115}In^{m}$	$1/2^{-}$	336 keV	4.49 h
$^{113}Cd^{m}$	$11/2^{-}$	263 keV	14.1 y
$^{85}Kr^{m}$	$1/2^{-}$	305 keV	4.48 h

Photoexcitation of isomers is verified by detecting photoneutrons. The $^{155}Gd^{m}$ isomers with the spin-parity of $11/2^{-}$ and the excitation energy 121 keV are photo-excited just above the neutron threshold at 6635 keV by a highly monochromatic gamma-ray beam with an energy spread 0.5% (33keV) in FWHM at energies between 6514 and 6635 keV. Thus, photoneutron emission occurs on ^{155}Gd not in the ground state but in the isomeric state. The neutron detection is carried out in collaboration with the research group "Gamma above Neutron Threshold".

2.1.2. Technical proposal

The proposed experiment of the production and photoexcitation of isomers requires the following preparatory Research and Development:

1) A preparatory investigation of laser acceleration of electrons with the 1 PW laser at the CETAL facility in Magurele. The peak power (1 PW) and pulse width of the laser need to be modified and optimized to accelerate electrons in the MeV region at high fluxes. A gas or solid target will be employed for this purpose (this will be defined in a common ELI-NP – CETAL research project).
2) Test for the production of isomers with the 1 PW laser at the CETAL facility. Production reactions of the inelastic electron scattering, (e, e' γ) and (e, e' n), as well as photoabsorption of the Bremsstrahlung photons, need to be investigated with emphasis on the production efficiency of isomers.

The fundamental technology developed by the preparatory investigation will be applied to the proposed experiment with the 10 PW laser and the gamma beam at the ELI-NP facility. In the E7 experimental area it will be possible to use also the 1 PW laser beam at 1 Hz repetition rate, transported through the 10 PW beamline(s). A long focal-length parabolic focusing mirror, housed in a turning box located in the E1/E6 experimental area, will allow for the use of the long focus (9.5 m) at 1 PW and 10 PW. This is beneficial for electron acceleration in a gas target, and specifically for this experiment we do not need very tight focus, a long focal being desirable (Figure 6).

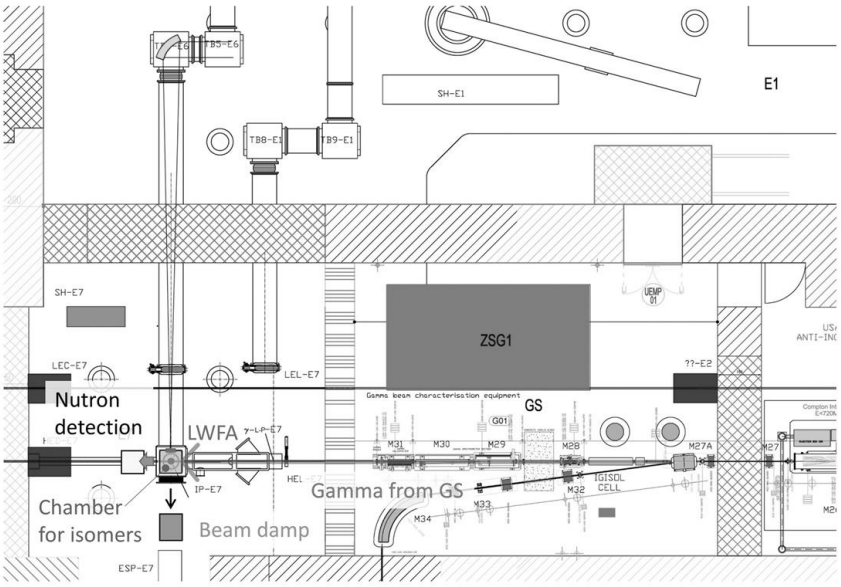

Figure 6 - Experimental setup of E7-Stage 1

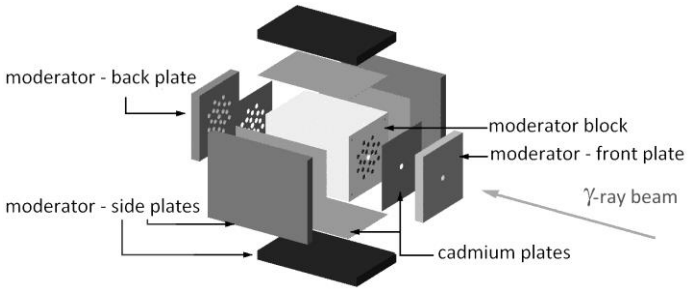

Figure 7 - Schematic image of the 4π neutron detector structure, proposed in the ELI-NP TDR "Gamma Above Neutron Threshold".

The electrons accelerated with the help of the high-power laser will hit a first target, of tungsten (W), to produce Bremsstrahlung radiation in the gamma domain. Then, at a distance that depending on the isomer to be studied and on the geometry of the electron acceleration and Bremsstrahlung setup may vary from a few mm to a few cm, there is the second target, containing the nucleus of interest. By irradiation with the Bremsstrahlung gamma-rays, part of the nuclei in this target will reach (by direct and more preferably indirect feedings) the isomeric state to be investigated.

At a next moment (after a delay depending on the lifetime of the isomeric state), the target is irradiated with the gamma beam from GBS with an energy tuned in such a way as to be slightly above the neutron threshold from the isomeric state (but not also from the ground state) and the photoneutrons are detected.

At ELI-NP foreseen is the presence of a 4π array for neutron detection, which is described in the "Gamma above Neutron Threshold" TDR (Figure 7). The procedure for the purchase of the ^{3}He detectors for this array already started. Depending on the results of the preparatory experiments, the detectors will be placed around the secondary (isomer) target, or a fast transport system will be installed to transport the target to the 4π array after the irradiation with the Bremsstrahlung gamma photons. In either case, the neutron detectors array will be placed on the gamma radiation beam from GBS (and the photoexcitation of the isomers created in the target shall occur when the target is in the 4π array).

2.1.3. Estimation Feasibility

There are several considerations that support the idea of performing this experiment at ELI-NP. One of them is the availability of an intense, narrow-bandwidth gamma radiation beam. Another one is the possibility to use high power lasers for accelerating electrons and put the nuclei in the isomeric states of interest.

The signal to noise ratio for neutron detection is greatly enhanced by the fact that only a small fraction of the time is covered by the gamma radiation pulses, the macrobunches occupying only approximately 50 μs each second.

Due to the fact that the production of isomeric states is expected to be more efficient with the help of gamma photons with respect to electron scattering, envisaged is the use of a Bremsstrahlung target placed immediately after the electron acceleration site (laser beam focus). In the lower panel of Figure 8, displayed are the results of the GEANT4 simulation of the Bremsstrahlung spectra originating from a W target on which 10^6 laser-accelerated electrons arrive with an energy of 40 MeV and an energy spread of 1%.

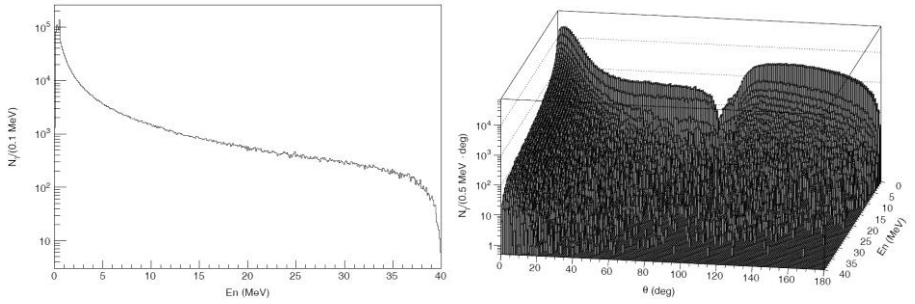

Figure 8 - Energy spectrum (left panel) and angular-energy distribution (right panel) of Bremsstrahlung gamma radiation photons exiting the primary W target.

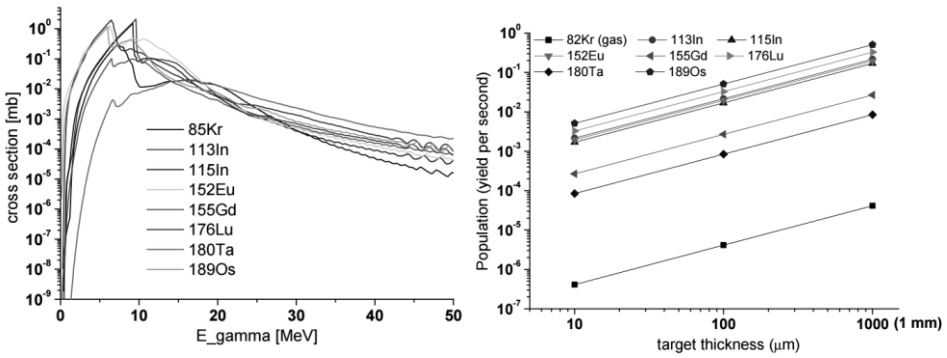

Figure 9 - Left panel: Total cross-section for the production of the isomers as computed with TALYS code. Right panel: population of the isomer state for three target thicknesses due to the irradiation with the Bremsstrahlung radiation with the characteristics in Figure 8.

The number of electrons accelerated with the help of 1 PW or 10 PW lasers can be estimated/extrapolated from previous experiments with existing, lower power lasers [7]. The number of electrons accelerated by a 1 PW laser pulse in the 50 MeV range can be 10^{10}, while for 10 PW this figure may be one order of magnitude higher.

Isomers are populated through photoexcitation of mediating states at higher excitation energies followed by gamma-transitions to the isomer. Considering only the photons exiting the W target at small angles (within 10^{o}) in the direction of the incident electrons, one can estimate the number of isomers produced per laser shot. In Figure 9 the population of the isomer state is presented for targets of widths of 10 μm, 100 μm and 1 mm and for 10^6 laser-accelerated electrons creating the Bremsstrahlung distribution in Figure 8.

Taking as an example the $^{176}Lu^{m}$ case, due to the quite large lifetime of the isomeric state, several 1 PW laser shots can be used in order to excite the target. For a 1-hour laser functioning, meaning a delivery of 3600 shots at 1 PW on target, and assuming a secondary ^{176}Lu target of 1 mm diameter on which consequently the 8×10^8 ph/s (within the bandwidth) gamma beam hits, a count rate of about 0.3 neutron/second is expected in the 4π detector. By using a gate of equal duration with the time (1 ms) needed for neutron moderation in the polyethylene for each gamma macro-bunch, the signal to noise ratio is improved by a factor of 10.

For the short-lived isomers, such as $^{155}Gd^{m}$ (32 ms), they can be produced by one shot of the 10 PW laser, then photo-excited by synchronized irradiations with a single-shot of gamma micro-bunch followed by neutron detection with fast Li glass scintillation detectors with a time gate 100 ns.

The preparatory experiments of laser acceleration of electrons aim to improve these numbers by increasing the electron yield and optimizing the geometry of the setup.

2.2. Search for sub-eV Dark Matter candidates at E4 (RA5-DM)

In this proposal we search for frequency up-shifted photons via four-wave mixing in the vacuum caused by stimulated decay of resonantly produced DM when two color lasers are combined and focused into the vacuum as illustrated in Figure 10. Figure 11 shows the experimental setup we propose at E4.

A large fraction of dark components in the universe motivates us to search for yet undiscovered fields to naturally interpret the relevant observations. Because we know examples of resonance states coupling to two photons at 126 GeV (scalar field, Higgs) and 135 MeV (pseudoscalar field, neutral pion) within only three orders of magnitude on the mass scale, we may expect that there might be yet undiscovered similar types of resonance states over much wider energy ranges in

nature, in particular, in the lower energy side if the coupling to two photons is so weak that these dark fields are not discovered by conventional methods to date. This encourages us to further search for resonance states at energy ranges below 1 MeV to which conventional charged particle colliders will never be able to access.

There are actually theoretical rationales to expect sub-eV particles such as the axion (pseudoscalar boson) [8] and the dilaton (scalar boson) [9] associated with breaking of fundamental symmetries in the context of particle physics and cosmology. Therefore, we are led to probe such fields via their coupling to two-photons in the sub-eV mass range. Furthermore, the advent of high-intensity laser systems and the rapid intensity growth encourage the approach to probe weakly coupling dark fields with optical photons by the enhanced luminosity factor [10, 11].

We therefore propose searches for resonantly produced dark fields with quasi-parallel two-color laser-laser collider at E4 where two 100 TW lasers are available and two 1 PW lasers will also be available if the beam transport at the upstream is slightly reconfigured.

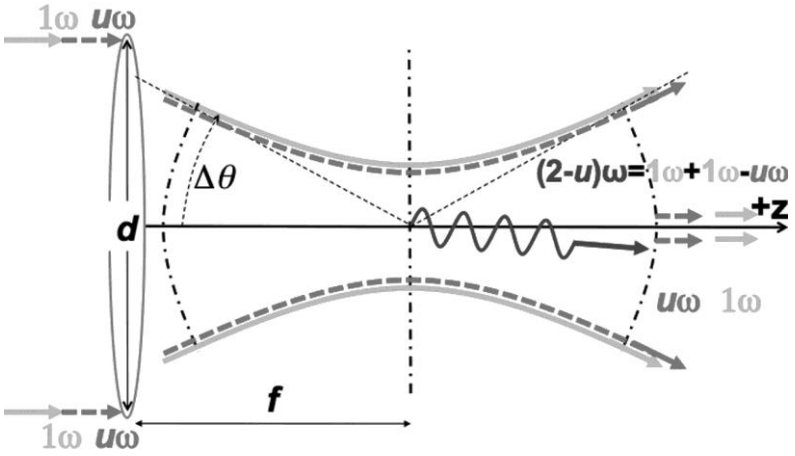

Figure 10 - Schematic view of quasi-parallel colliding system (QPS) between two incident photons among a focused laser beam with the focal length *f*, the beam diameter *d*, and the upper range of incident angles $\Delta\theta$ determined by geometric optics. The signature $(2-u)\,\omega$ is produced via the four-wave mixing process, $1\omega + 1\omega \rightarrow (2-u)\,\omega + u\,\omega$ with $0 < u < 1$ by mixing two-color waves with different frequencies 1ω and $u\,\omega$ in advance at the incidence.

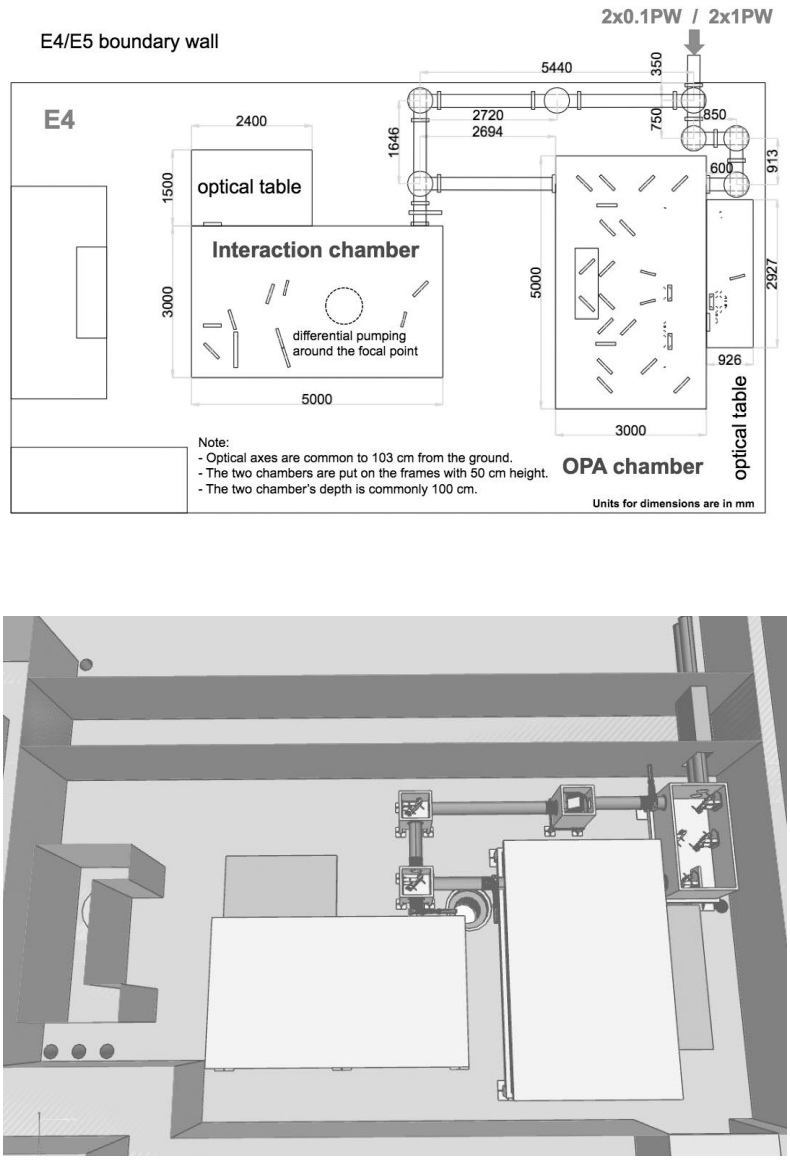

Figure 11 - Arrangement of the basic components for the setup and the CAD drawing at E4 to search for sub-eV Dark Matter via four-wave mixing in the vacuum.

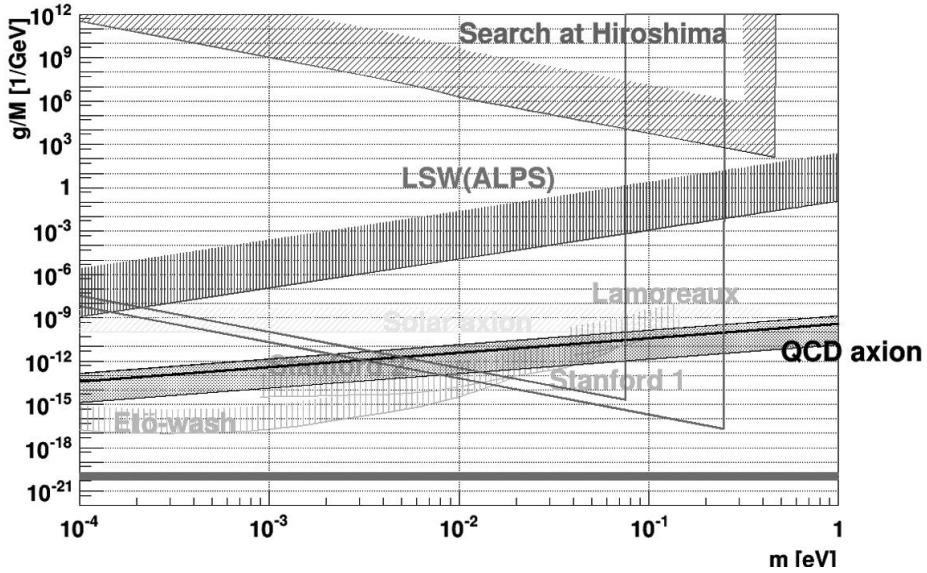

Figure 12 - Upper limits on the coupling *g/m*- mass m relation for the scalar field exchange. As references in Figure 12, we put existing upper limits by our pilot search (Search at Hiroshima) based on this method [12] and also by the other types of scalar field searches by vertically shaded areas: the ALPS experiment [13] (the sine function part of the sensitivity curve is simplified by unity for the drawing purpose) which is one of the "Light Shining through a Wall" (LSW) experiments, searching for non-Newtonian forces based on the torsion balance techniques (Etö-wash [14], Stanford1 [15], Stanford2 [16]) and the Casimir force measurement (Lamoreaux [17]). The domains below the vertically shaded areas are all excluded. We note that if we require the proper polarization combinations between initial and final states for pseudoscalar fields [10], we will be able to test the QCD axion models in the near future. As a reference, we show the expected mass-coupling relation based on the QCD axion scenario for E/N = 0 [18] (KSVZ model [19]) which is indicated by the inclining dotted line. The pink horizontal line indicates the gravitational coupling limit.

Goal of this research: Even if no statistically significant four-wave mixing signal is observed, it is possible to constrain fundamentally important theoretical models for Dark Matter such as Quantum Chromodynamics (QCD) axion scenarios based on the mass-coupling relation of the exchanged fields as shown in Figure 12. The accessible domains by the searches at ELI-NP are indicated by the two red lines from the top to the bottom for cases where 0.1 PW with an OPA-based inducing laser and 1 PW with an OPA-based inducing laser are assumed, respectively. The assumed data taking periods are commonly about 10 days. The red lines indicate that ELI-NP has the potential to test QCD axion scenarios in the

mass range 1−100 meV, corresponding to a sensitivity beyond the present world record.

2.3. R&D for Gamma-Polari-Calorimeter (RA5-GPC)

Gamma Polari-Calorimeter (GPC) is the common detector system that will be employed in Stage 1.5 and 3 at E7 as illustrated in conceptual drawing (Figure 13) and CAD drawing (Figure 14).

GPC is designed to measure incident gamma-ray energies via the conversion process to e^+e^- pairs and simultaneously measures the degree of linear polarization. The energy and polarization of gamma-rays are determined by the pairwise reconstruction on the basis of one-by-one tracking of electrons and positrons. Therefore, a part of GPC is also applicable to a spectrometer of e^+ and e^- individually without the gamma-conversion target.

GPC has capabilities of measuring ten pairs per shot and covering the energy range of 0.1−5.0 GeV. The inclusive momentum resolution of GPC for e^+ and e^- above 0.2 GeV is 6.5% (Figure 15), assuming incident gamma-ray energy is 1.0 GeV.

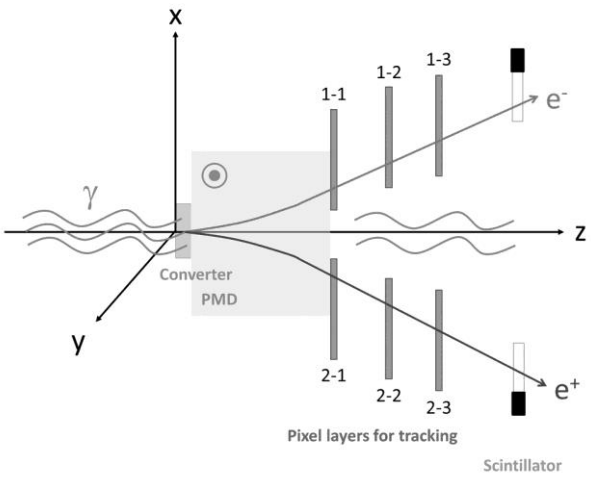

Figure 13 - Conceptual drawing for Gamma Polari-Calorimeter (GPC). Note that the typical e^+e^- opening angle is around sub-mrad. The angle at the top-view is exaggerated.

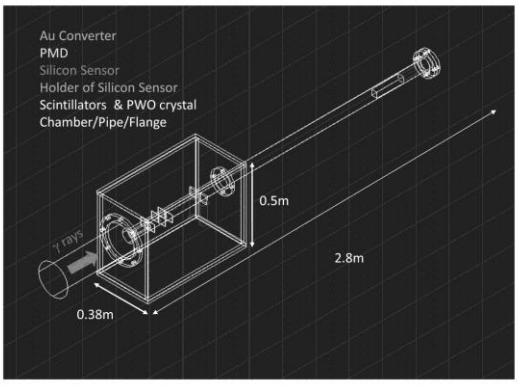

Figure 14 - A CAD drawing for GPC.

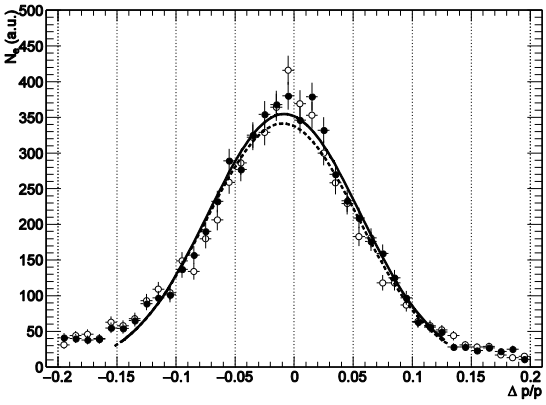

Figure 15 - Inclusive momentum resolution of produced e^+ (closed circle) and e^- (open circle) above 0.2 GeV.

3. STAGE 1.5

In this setup, we will investigate radiation reaction (RA5-RR), e^-e^+ pair production (RA5-Pair) and polarization (RA5-Pol) at E7. We can carry out these 3 experiments simultaneously, therefore the considered experimental setup in this stage is only one configuration (Table 4 and Figure 16).

Table 4
Parameters for experiments

Electron source	energy [MeV]	bunch size [μm]	Laser energy [J]	Intensity [W/cm^2]	duration [fs]	spot size [μm]
accelerator	600	15	220	(1-2)×10^{22}	22	5.6

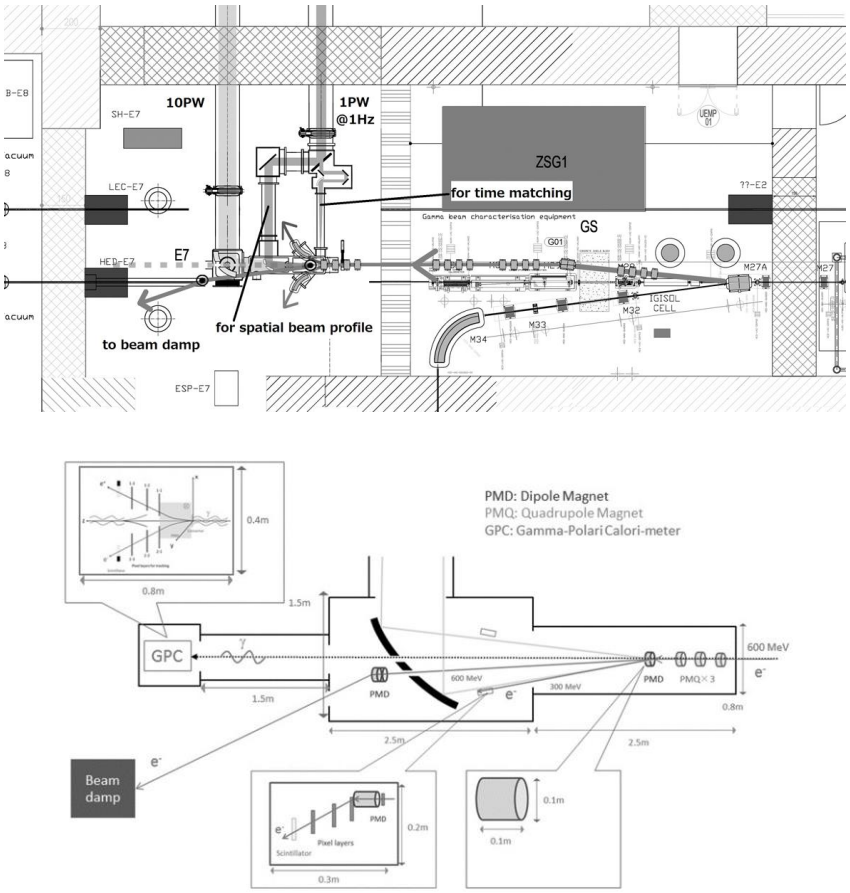

Figure 16 - Experimental setup of E7-Stage 1.5.

3.1. Radiation Reaction

3.1.1. Introduction/Physics Case

The following descriptions of the physics case are partially based on the recent publication [20] by the author of this section. That paper was intended to propose very briefly an experiment for ELI-NP including the theoretical explanations. And also we extracted the proposal of RA5-RR from Technical Design Report for Research Activity 5 – Combined Laser and Gamma Experiments (RA5-TDR) after adding new information for this present paper.

Ultrahigh intense lasers are being planned and constructed [21] including ELI-NP [22]. What kind of physical processes can we observe in the regime of these laser intensities? We often discuss QED effects like pair creation/annihilation by extreme intensities of 10^{24} W/cm^2 [22]. It has been predicted that these lasers will produce new high-field physics. Before reaching this physical process, we need to pass through the region of $10^{21} - 10^{22}$ W/cm^2. In this regime, it is predicted that an electron will emit significant energy as light. Therefore, the motion of the electron needs to be corrected by the radiation feedback [23, 24]. This is a basic physical process, named "radiation reaction (RR)". This effect will be appear in the regime of this laser intensities. All materials have electrons in atoms, and the part of these will be freed from the potential of atoms, then they emit strong light via the interaction with the high-intensity fields. Therefore, the RR process becomes very important for all experiments with ultra-intense lasers at intensities over 10^{22} W/cm^2.

These intensities are enough reasonable to aim by using ELI-NP two 10 PW lasers. In our group RA5-TDR considers to use E7 experimental area in ELI-NP, we can use the two 10 PW lasers and the electron LINAC (max 720 MeV) for gamma-ray sources here. By combining these large devices, we intend to carry out to examine radiation reaction (RA5-RR), pair creation (RA5-Pair), observing polarization of radiation (RA5-Pol) and vacuum birefringence (RA5-VBir) under the high-intensity laser fields. In this chapter, we present the detail of our proposal for the RA5-RR experiment in RA5-TDR (HPLS-TDR3) group.

Although many readers may indeed argue that this is very obvious and basic physics, however the RR remains one of the difficult problems in the basic equation of a radiating electron motion, namely "run-away" as an instability of its self-acceleration. The standard theory of it was formulated by Lorentz [25], Abraham [26] and Dirac [27]. Therefore, the equation of a radiating electron motion is named the "Lorentz-Abraham-Dirac" (LAD) equation. The easiest way to derive this equation is, from the radiation energy loss formula (Larmor's formula [28]) in the non-relativistic regime [29, 30].

$$\left.\frac{dE}{dt}\right|_{\text{non-relativistic}} = -m_0\tau_0\left(\frac{d\mathbf{v}}{dt}\right)^2 \tag{3.1.1}$$

Where, m_0 is the electron rest mass, $\mathbf{v} \in \mathrm{E}^3$ is the velocity of the electron (E^3 is a 3-dimensional Euclidian space). c is denoted as the speed of light, $\tau_0 = e^2/6\pi\varepsilon_0 m_0 c^3 = O(10^{-24})$. Therefore, the energy change of an electron is as follows ($\mathbf{F}_{\text{ex}} \in \mathrm{E}^3$ is an external field.):

$$\frac{d}{dt}\left(\frac{m_0\mathbf{v}^2}{2}\right) = \mathbf{F}_{\text{ex}}\cdot\mathbf{v} - m_0\tau_0\left(\frac{d\mathbf{v}}{dt}\right)^2. \tag{3.1.2}$$

From this equation, we can obtain the equation of motion named the Lorentz-Abraham (LA) equation.

$$m_0\frac{d\mathbf{v}}{dt} = \mathbf{F}_{\text{ex}} + \mathbf{F}_{\text{LA}} \tag{3.1.3}$$

$$\mathbf{F}_{\text{LA}} = m_0\tau_0\frac{d^2\mathbf{v}}{dt^2}. \tag{3.1.4}$$

Here, our dynamics is in $t \in [t_{\text{initial}}, t_{\text{final}}] \subset \mathrm{R}$ with the periodic conditions in which

$$\mathbf{v}(t_{\text{initial}}) = \mathbf{v}(t_{\text{final}}), \quad \frac{d\mathbf{v}}{dt}(t_{\text{initial}}) = \frac{d\mathbf{v}}{dt}(t_{\text{final}}) \tag{3.1.5}$$

are required. Equation (3.1.4) is the effect of RR, named "the RR force". Equation (3.1.3) with (3.1.4) was converted to the relativistic regime by Dirac without any mathematical condition like Eq. (3.1.5). This is the LAD equation.

$$m_0\frac{d}{d\tau}w^\mu = -eF_{\text{ex}}^{\mu\nu}w_\nu + {f_{\text{LAD}}}^\mu \tag{3.1.6}$$

$${f_{\text{LAD}}}^\mu = \frac{m_0\tau_0}{c^2}\left(\frac{d^2w^\mu}{d\tau^2}w^\nu - \frac{d^2w^\nu}{d\tau^2}w^\mu\right)w_\nu \tag{3.1.7}$$

where all of vectors in this equation belong to the 4-dimensional linear vector space ${\mathrm{V}_{\mathrm{M}}}^4$ joining in Minkowski spacetime (A^4, g) which is the mathematical set of the 4-dimensional affine space A^4 and the Lorentz metric g with the signature of $(+,-,-,-)$. The force of $f_{\text{LAD}} \in {\mathrm{V}_{\mathrm{M}}}^4$ is the effect of the radiation feedback, denoted the RR force.

At first, the LAD theory is developed as the electron's model in classical dynamics instead of the Dirac equation for avoiding the infinity in QED. After that it was solved via renormalization [31-33], but he had tried to apply the Lorentz model (1906) [25] for that. A part of an electron with the spherical charge distribution interacts with other parts of itself. But, the field at the center of this charge becomes a singular point (since $|\mathbf{E}| \propto r^{-2}$, $r \to 0 \Rightarrow |\mathbf{E}| \to \infty$). We need to keep in mind that the electron is treated as a point charge in classical physics. This dependence is taken over the electromagnetic mass,

$$m_{\mathrm{EM}} = \frac{3}{4}\frac{\tau_0 c}{r} m_0 \overset{r\to 0}{\to} \infty . \tag{3.1.8}$$

In the Lorentz's theory, RR is derived from only the retarded field [34, 35]. The equation of electron's motion (Eq. (3.1.3) with Eq.(3.1.4)) becomes

$$\left(m_0 + m_{\mathrm{EM}}\right)\frac{d\mathbf{v}}{dt} = -e\left(\mathbf{E} + \mathbf{v}\times\mathbf{B}\right) + m_0\tau_0\frac{d^2\mathbf{v}}{dt^2} . \tag{3.1.9}$$

Dirac considered that the infinity of QED is equivalent to the infinity of the electromagnetic mass [36]. In Dirac's method, he treated not only the retarded field, but also the advanced field [27]. Then, the equation which he obtained is the LAD equation (3.1.6) with Eq. (3.1.7). However, these equations have a mathematical difficulty which is named "run-away". For instance, we consider the case without any external fields. In this case,

$$\begin{aligned} &\left(m_0 + m_{\mathrm{EM}}\right)\frac{d\mathbf{v}}{dt} = m_0\tau_0\frac{d^2\mathbf{v}}{dt^2} \\ \Leftrightarrow\quad &\frac{d\mathbf{v}}{dt}(t) \propto \frac{d\mathbf{v}}{dt}(0)\times\exp\left(\frac{m_0 + m_{\mathrm{EM}}}{m_0}\frac{t}{\tau_0}\right). \end{aligned} \tag{3.1.10}$$

Here, τ_0 is a very small value with the order of 10^{-24} sec, the solution grows up rapidly since t/τ_0 is significant due to the second order derivative $m_0\tau_0 d^2\mathbf{v}/dt^2$, namely the Schott term. This self-accelerating effect is the run-away solution which we need to avoid. The same problem is in the LAD equation, too. RR has involved the history of the single electron model on how to avoid the run-away and the concrete problem how to estimate this effect under the interactions between ultrahigh-intensity lasers and highly energetic electrons in many ELI-NP experiments.

As we discussed above, we need to investigate the method of the solution for the run-away problem for the estimation of the count-rates for the PW class laser experiments like ELI-NP. In this small section, we pick up some useful method for RR researches.

For the avoidance of run-away solution, many methods have been proposed and used for simulations like PIC. The standard method for the avoidance of run-away was suggested by Eliezer, Ford-O'Connel and Landau-Lifshitz. They considered the term of the RR force as the higher order corrections. Therefore, the RR force term is treated by the first order of perturbations. By replacing the Schott term $m_0 d^2 w^\mu/d\tau^2$ with $d(-eF_{\mathrm{ex}}^{\mu\nu} w_\nu)/d\tau$ in the radiation reaction force,

$$m_0\frac{d}{d\tau}w^\mu = -eF_{\mathrm{ex}}^{\mu\nu} w_\nu - \frac{\tau_0 e}{c^2}\left[\frac{d(F_{\mathrm{ex}}^{\mu\theta} w_\theta)}{d\tau}w^\nu - \frac{d(F_{\mathrm{ex}}^{\nu\theta} w_\theta)}{d\tau}w^\mu\right]w_\nu \tag{3.1.11}$$

derived by Eliezer [37] and Ford-O'Connel [38]. For PIC simulations, the external fields is the function of spacetime, $F_{\mathrm{ex}} = F_{\mathrm{ex}}(x(\tau)) \in \mathrm{V_M}^4 \otimes \mathrm{V_M}^4$. Using the chain

rule of derivative in Eq. (3.1.11), we can obtain the force of Landau-Lifshitz equation [39]:

$$m_0 \frac{d}{d\tau} w^\mu = -eF_{\text{ex}}^{\mu\nu} w_\nu - \frac{\tau_0 e}{c^2} w^\lambda w_\nu \partial_\lambda F_{\text{ex}}^{\mu\nu} + \frac{\tau_0 e^2}{c^4 m_0} \left(c^2 F_{\text{ex}}^{\mu\nu} F_{\text{ex}\,\nu\lambda} w^\lambda + F_{\text{ex}}^{\mu\nu} F_{\text{ex}\,\mu\lambda} w_\nu w^\lambda w^\mu \right). \tag{3.1.12}$$

Of course, $f_{\text{ex}} \in \mathrm{V_M}^4$ is an external force defined by $f_{\text{ex}}^\mu = -eF_{\text{ex}}^{\mu\nu} w_\nu$. Since this method doesn't have a run-away due to the absence of the Schott term, it is useful for the reference of simulations. A scheme similar to this was obtained by Rohrlich [40].

Another method is to use the Sokolov equation. This is similar to Landau-Lifshitz equation (3.1.12), but it can be installed the radiation spectrum. For example, we can obtain the following equations when we choose the classical radiation spectrum.

$$\frac{dp^\mu}{d\tau} = -eF_{\text{ex}}^{\mu\nu} \frac{dx_\nu}{d\tau} - \frac{I_{\text{cl}}}{{m_0}^2 c^2} p^\mu \tag{3.1.13}$$

$$\frac{dx^\mu}{d\tau} = \frac{p^\mu}{m_0} + \frac{\tau_0 f_{\text{ex}}^\mu}{m_0} \,. \tag{3.1.14}$$

Here, $I_{\text{cl}} = -\tau_0 / m_0 \times g_{\mu\nu} f_{\text{ex}}^\mu f_{\text{ex}}^\nu$ means the classical radiation (the Larmor's formula) [41]. Then, we consider QED-based radiation formula $I_{\text{QED}} = q(\chi) \times I_{\text{cl}}$ with

$$q(\chi) = \frac{9\sqrt{3}}{8\pi} \int_0^{\chi^{-1}} dr\, r \left[\int_{r_\chi}^{\infty} dr' K_{5/3}(r') + \chi^2 r r_\chi K_{2/3}(r_\chi) \right], \tag{3.1.15}$$

$\lambda\!\!\!^{-}_C = \hbar / m_0 c$, $\chi = 3/2 \times \lambda\!\!\!^{-}_C / m_0 c^2 \times (-g_{\mu\nu} f_{\text{ex}}{}^\mu f_{\text{ex}}{}^\nu)^{1/2}$ and $r_\chi = r/(1-\chi r)$. This result was derived from QED calculation [42, 43]. By using this QED-based radiation formula, He proposed the upgraded equations [44]:

$$\frac{dp^\mu}{d\tau} = eF_{\text{ex}}^{\mu\nu} w_\nu + \frac{I_{\text{QED}}}{{m_0}^2 c^2} p^\mu \tag{3.1.16}$$

$$\frac{dx^\mu}{d\tau} = \frac{p^\mu}{m_0} + \frac{I_{\text{QED}}}{I_{\text{cl}}} \frac{\tau_0 f_{\text{ex}}^\mu}{m_0} \tag{3.1.17}$$

Characteristics of this model are, (1) it can realize the main behavior of a radiating electron by QED-based radiation and (2) the fact that the equations satisfy the relation $p_\mu p^\mu = (m_0 c)^2$ but don't satisfy $w_\mu w^\mu = c^2$. The latter point should be discussed on the mathematical point of view.

One of the authors in this paper, Seto has also suggested a series of new models, based on the propagation of fields in the QED vacuum fluctuation proposed by Heisenberg and Euler, in another word as the correction of vacuum

permittivity ε_0 . By correcting radiation from electron via the QED vacuum fluctuation (the modified propagation of photons), we can derive the equation, namely the Seto-Zhang-Koga (SZK) equation,

$$\frac{d}{d\tau}w^{\mu} = -\frac{e}{m_0[1-\eta f(F_{\mathrm{LAD}})]}\left(F_{\mathrm{ex}}^{\mu\nu} + F_{\mathrm{LAD}}{}^{\mu\nu}\right)w_{\nu} \tag{3.1.18}$$

$$F_{\mathrm{LAD}}\big|_{x=x(\tau)} = -\frac{m_0\tau_0}{ec^2}\left(\frac{d^2w}{d\tau^2}\otimes w - w\otimes\frac{d^2w}{d\tau^2}\right) \tag{3.1.19}$$

($\eta = 4\alpha^2\hbar^3\varepsilon_0/45{m_0}^4c^3$ and $f(F) = \langle F \mid F\rangle$ defined by $\langle A \mid B\rangle = A_{\alpha\beta}B^{\alpha\beta}$) [20, 45]. Then, this equation was upgraded to the "Seto I" model as follows [46]:

$$d\mathsf{m}\frac{dw^{\mu}}{d\tau} = -d\mathsf{E}^{\mu\nu\alpha\beta}\mathsf{F}_{\alpha\beta}w_{\nu} \tag{3.1.20}$$

$$\frac{d\mathsf{E}^{\mu\nu\alpha\beta}}{d\mathsf{m}} = \frac{e}{m_0[1-\eta f(\mathsf{F})]}\left[g^{\mu\alpha}g^{\nu\beta} + \eta g(\mathsf{F})\times\frac{\varepsilon^{\mu\nu\alpha\beta}}{2!}\right]. \tag{3.1.21}$$

Here, $g(F) = 7/4\times\langle F \mid {*F}\rangle$ and ${*F} \in \mathrm{V_M}^4 \otimes \mathrm{V_M}^4$ means the dual tensor of F . We should note that $d\mathsf{E}^{\mu\nu\alpha\beta}$ and $d\mathsf{m}$ are the measure for the charge and the mass on the Minkowski spacetime (A^4, g) , satisfying $d\mathsf{E}^{\mu\nu\alpha\beta} = d\mathsf{E}^{\mu\nu\alpha\beta}/d\mathsf{m}\times d\mathsf{m}$. $\mathsf{F} = F_{\mathrm{ex}} + F_{\mathrm{LAD}}$ and it includes radiation-external field interactions via $\langle F_{\mathrm{LAD}} \mid F_{\mathrm{ex}}\rangle$ and $\langle F_{\mathrm{LAD}} \mid {*F_{\mathrm{ex}}}\rangle$. In addition, it proceeded the more general model including QED-based synchrotron formula characterized by Eq. (3.1.15) (Seto II model [47]):

$$d\mathsf{m}\frac{dw^{\mu}}{d\tau} = -d\mathsf{E}^{\mu\nu}{}_{\alpha\beta}\mathsf{F}_{\mathrm{hom}}{}^{\alpha\beta}w_{\nu} \tag{3.1.22}$$

$$\frac{d\mathsf{E}^{\mu\nu\alpha\beta}}{d\mathsf{m}} = \frac{e}{m_0}\frac{[1-\eta f(\mathsf{F}_{\mathrm{hom}})]\times g^{\mu\alpha}g^{\nu\beta} + \eta g(\mathsf{F}_{\mathrm{hom}})\times\dfrac{\varepsilon^{\mu\nu\alpha\beta}}{2!}}{[1-\eta f(\mathsf{F}_{\mathrm{hom}})]^2 + [\eta g(\mathsf{F}_{\mathrm{hom}})]^2} \tag{3.1.23}$$

$$F_{\text{Mod-LAD}}\big|_{x=x(\tau)} = -\frac{m_0\tau_0}{ec^2}\left[\frac{d^2(\Xi w)}{d\tau^2}\otimes w - w\otimes\frac{d^2(\Xi w)}{d\tau^2}w\right] \tag{3.1.24}$$

$\mathsf{F}_{\mathrm{hom}} = F_{\mathrm{ex}} + F_{\text{Mod-LAD}}$ is the homogeneous field. When $\Xi = I_{\mathrm{QED}}/I_{\mathrm{cl}} = q(\chi)$, this set of equations behaves dynamically similar to Eqs. (3.1.16)- (3.1.17) [47]. These models demonstrated the stability of their solutions, and became good references.

ELI-NP has the potential for carrying out relevant experiments of RR, with the help of the two 10 PW - over 10^{22} W/cm^2 class lasers and the Gamma-ray Source - LINAC (GS-LINAC) for highly energetic electron bunches. Moreover, RR has to be taken into account in all high intensity laser experiments. The recent models using QED modification show us the running coupling between an electron and radiation field in high-intensity fields. Therefore, this proposal is not only for

the investigation of the energy loss of a radiating electron, but we may also observe the running coupling of an electron dE by high-fields via the function $q(\chi)$ [see Eq. (3.1.15)]. The experiments of RR will give us a chance to consider the problem of laser-electron interactions and the physics of an electron model like the Dirac's original prospect.

We propose the experimental geometries of the head-on collision between a 10 PW laser beam and 600 MeV / 2.5 GeV / 5.0 GeV electrons for the RR experiments in ELI-NP. Figure 17 is one of the setups for RA5-RR, combining the electrons from the GBS LINAC (on a new transport line to E7) and 10 PW laser beam, in Stage 1.5. We will discuss the technical details in Sect. 3.1.2. This experiment is based on the observation of two parameters: the minimum energy of scattered electron/shot and the maximum value of the photon energy. By the correlation of these two values, one can understand the dynamics of RR.

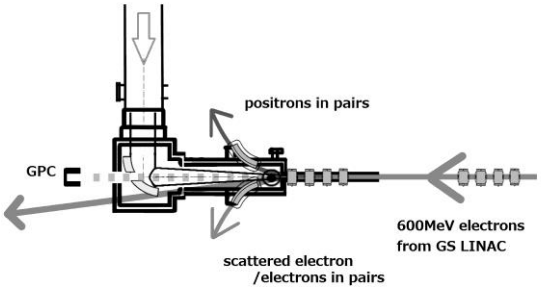

Figure 17 - Conceptual layout of RA5-RR in Stage 1.5. It will be carried out by the combination of the 10 PW laser and the GS-LINAC.

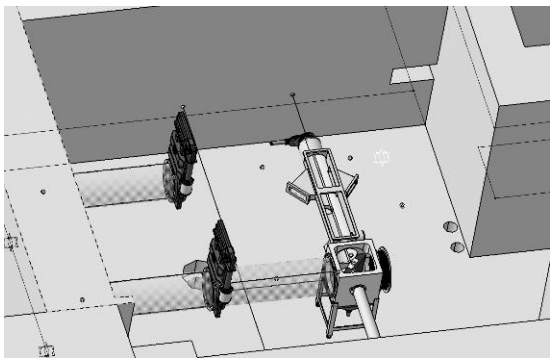

Figure 18 - 3D layout of RA5-RR/Pair/Pol experiments in Stage 1.5.

3.1.2. Technical Proposal

Before exceeding the numerical results, we provide the experimental setup as the conclusion of them. From the simulation results, we will classify the models of radiation reaction (RR) by using a head-on laser-electron interaction. We also use this setup as the common configuration for RA5-Pair and RA5-Pol experiments. We need to observe the minimum energy of the scattered electrons and the maximum energy of the emitted photons from the electrons. The sketch of this E7 area is Figure 18 and Figure 19. For this setup, a basic requirement is the synchronization between the 600 MeV electron bunches from the GS-LINAC and the 10 PW laser pulses, at the sub-ps level. These are also important in the alignment stage of the setup. In the development contracts for the two 10 PW laser system and the Gamma Beam System at ELI-NP, there is already foreseen the possibility of synchronization at the 100 fs level. In addition, we propose these experiments in E7-Stage 3 employing Laser WakeField Acceleration (LWFA) for 2.5 / 5.0 GeV electron beams, to enter another regime of highly intense field physics.

In the following we present the elements that form a functional experimental setup for this physics case (also for the LWFA case). These elements are also common equipment for other physics cases proposed in the TDR.

The setup is illustrated in Figure 19. We consider to use the electron bunches from GS-LINAC at M27A magnet in this figure. By using the GS-LINAC, it is expected a very good beam profile of the electron bunches. Since we consider to pick up it at the front end of LINAC, the expected electron energy will go up 600-720 MeV. Here, we choose 600 MeV for an electron energy.

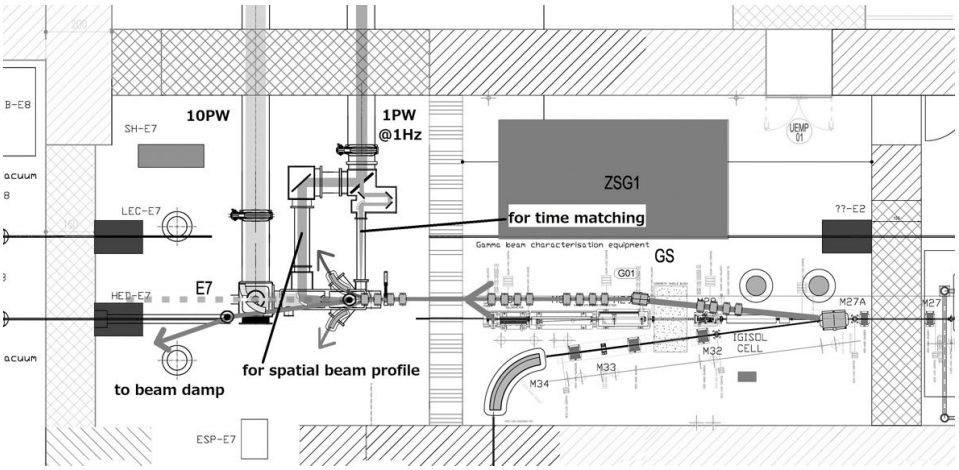

Figure 19 - Combined 10PW-Laser and GS-LINAC system.

We consider the following setup as the minimum requirement for the investigations of RR in ELI-NP. By following the paper of [23, 24], we aim the laser intensity of 10^{22} W/cm^2 by the focusing of a single arm of 10 PW. The purpose of this experiment is the confirmation of the theoretical model which described in the previous section. Especially, the QED modification of Eqs. (3.1.15)- (3.1.17) and (3.1.22) - (3.1.24) follow the analysis based on the Volkov solution [48]. This solution assumes that the external field should be the plane-wave, the strong focusing may violate these models. We select the f-number of 10 PW laser as $f^{\#} = 7$ with the focal length of 3 m due to this. With this focusing, the spot size is equal to 5.6 μm and the estimated range of the laser intensity is (1-2) × 10^{22} W/cm^2 depending on its peak power of 5-10 PW. The other parameters of the 10 PW laser are basically the standard ones for ELI-NP. The pulse energy, pulse duration and laser wavelength are 220 J, 22 fs and 820 nm respectively. This PW-class laser beam enters from E6 area to E7 and is reflected and focused by the final mirror. Then the beam direction becomes the one of the electron bunches extracted from the GBS-LINAC line.

For the experiments for the study of RR, the electron energy of 600 MeV is required, at a repetition rate at M27A magnet of 1 Hz (in case of using the 1 PW at 1 Hz laser beam, 0.016 Hz for the 10 PW beam). This repetition rate makes radiation safety issues much easier to solve. The charge in the bunch is estimated the range of 4.5 – 100 pC with 10^9 – 10^{10} electrons and the bunch width of 100 μm. Due to the statistics of the scattering processes, a well-focused electron beam at the interaction point is required. We take into consideration a beam size of 15 μm. Depending on the design of the extraction line from M27A magnet, we have the option of additional electron optics or accelerator modules.

Then an important subject is the synchronization between the 10 PW laser beam and the LINAC electron bunches. From the facility point of view, both HPLS and GBS systems foresee the possibility of external electronic synchronization.

We also need to align the electron beam profile with the laser beam with high precision. We thus propose the optical synchronization/alignment system in E7. There are two arms of the 10 PW lasers in E7, but for the alignment purposes it would be beneficial to have available the lower power 1 PW pulses at the higher repetition rate of 1 Hz. A part of this 1 PW is used for making 90 degree Compton scattering with electron bunches from LINAC. If the two arms of the laser are synchronized, with these scheme we can also set the time matching between the 10 PW beams and the LINAC. During the preparations for the experiments, we lead the remaining portion of the 1 PW – 1 Hz beam to collide head-on with the electron bunches, in order to scan the electron beam profile. The final focusing mirror for this will be located on moving stage remotely controlled for the scanning of the beam profile.

3.1.3. Estimation of Count Rate

In RA5-RR, the most interesting point is the choice of appropriate RR model in the regime of ELI-NP. Table 5 is the list of models which we consider in the present phase, the where symbols LL, CSok, QSok, SZK and Seto II stand for Landau-Lifshitz [39], Sokolov (classical) [41], Sokolov (quantum) [44], Seto-Zhang-Koga models [45] and the Seto II model [47] respectively. We have performed numerical simulations for tracking a radiating electron and the radiation spectrum in order to evaluate the model dependency of laser-beam interactions. In the spectrum estimation, the quantum emission spectrum [42] is employed for SQ and Seto II models while the classical emission spectrum [29] is used for the other models.

Table 5
Models of RR. The hatched columns include the QED-based modifications.

Model name	Equation
Landau-Lifshitz [LL], Eq. (3.1.12)	$m_0 \frac{d}{d\tau} w^\mu = -eF_{\rm ex}^{\mu\nu} w_\nu - \frac{\tau_0 e}{c^2} w^\lambda w_\nu \partial_\lambda F_{\rm ex}^{\mu\nu} + \frac{\tau_0 e^2}{c^4 m_0}(c^2 F_{\rm ex}^{\mu\nu} F_{{\rm ex}\,\nu\lambda} w^\lambda + F_{\rm ex}^{\mu\nu} F_{{\rm ex}\,\mu\lambda} w_\nu w^\lambda w^\mu)$
Sokolov (classical) [CSok], Eqs. (3.1.13)-(3.1.14)	$\frac{dp^\mu}{d\tau} = -\frac{e}{m_0} g_{\nu\theta} F_{\rm ex}^{\mu\nu}(p^\theta + \tau_0 f_{\rm ex}^\theta) - \frac{I_{\rm cl}}{m_0{}^2 c^2} p^\mu$
Sokolov (quantum) [QSok], Eqs. (3.1.16)-(3.1.17)	$\frac{dp^\mu}{d\tau} = -\frac{e}{m_0} g_{\nu\theta} F_{\rm ex}^{\mu\nu}[p^\theta + q(\chi)\tau_0 f_{\rm ex}^\theta] - \frac{q(\chi) I_{\rm cl}}{m_0{}^2 c^2} p^\mu$
Seto-Zhang-Koga [SZK], Eqs.(3.1.18) -(3.1.19)	$\frac{d}{d\tau} w^\mu = -\frac{e}{m_0[1-\eta f(F_{\rm LAD})]}(F_{\rm ex}^{\mu\nu} + F_{\rm LAD}{}^{\mu\nu}) w_\nu$
Seto II [Seto II] Eqs.(3.1.22) -(3.1.24)	$\frac{dw^\mu}{d\tau} = -\frac{e}{m_0} \frac{\left\{ \begin{array}{l} [1-\eta f(F_{\rm hom})] \times F_{\rm hom}{}^{\mu\nu} \\ +\eta g(F_{\rm hom}) \times {}^*F_{\rm hom}{}^{\mu\nu} \end{array} \right\}}{[1-\eta f(F_{\rm hom})]^2 + [\eta g(F_{\rm hom})]^2} w_\nu$

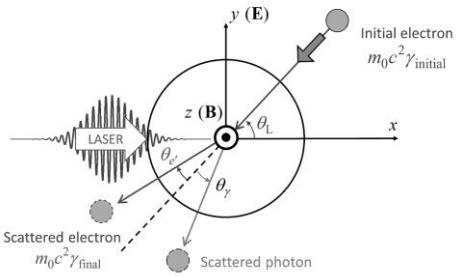

Figure 20 - Configuration of an electron scattering by a pulse laser.

We consider the following experiments: the peak intensity of the laser is $I = 1.0 \times 10^{22}$ W/cm^2 by spot size $S_P = 5.6$ μm for 5 PW with pulse duration $T_P = 22$ fsec and wavelength $\lambda = 820$ nm . The incident electron energy is $E = 600$ MeV provided by LINAC. Figure 20 is a diagram illustrating the configuration of electron scattering along with the definition of relevant angles: electron incident angle θ_L , electron scattering angle θ_e , and photon detection angle θ_γ .

Figures 21 and 22 show the electron orbits and the time evolution of electron energy calculated based on SZK, LL, CSok, QSok and Seto II models. Here, the case of the head-on collision, i.e., $\theta_L = 0^\circ$, is considered. As shown in Figure 21, the incident electron starts to oscillate under the action of laser electromagnetic field as it approaches the pulse laser. The electron tends to decelerate toward the direction of laser propagation ($+x$ direction) during the oscillation by light pressure. The electron eventually exhibits different dynamics according to the employed RR model and passes away into the distance with a certain scattering angle. As shown in Figure 22, the electron energy decreases drastically due to RR during the oscillation phase. The asymptotic value of electron energy considerably depends on the employed RR models. Scattered electron energy is estimated for various beam incident angles θ_L . We recognize two model groups from the final energies of an electron. The three models of LL, CSok and SZK are overlapped each other. And also QSok and Seto II are overlapped.

Figure 23 shows the scattered electron energy as a function of incident electron angle for each RR model. The electron energy decreases considerably from the initial beam energy, 600 MeV, due to radiation damping in any incident angles. Typical electron energy loss ranges from approximately 300 MeV for QSok and Seto II model to approximately 400 MeV for SZK, LL and CSok model. Therefore, evidence of RR could be observed from the scattered electron energy. In

addition, dependency of scattered electron energy on RR model becomes obvious as the incident angle becomes large.

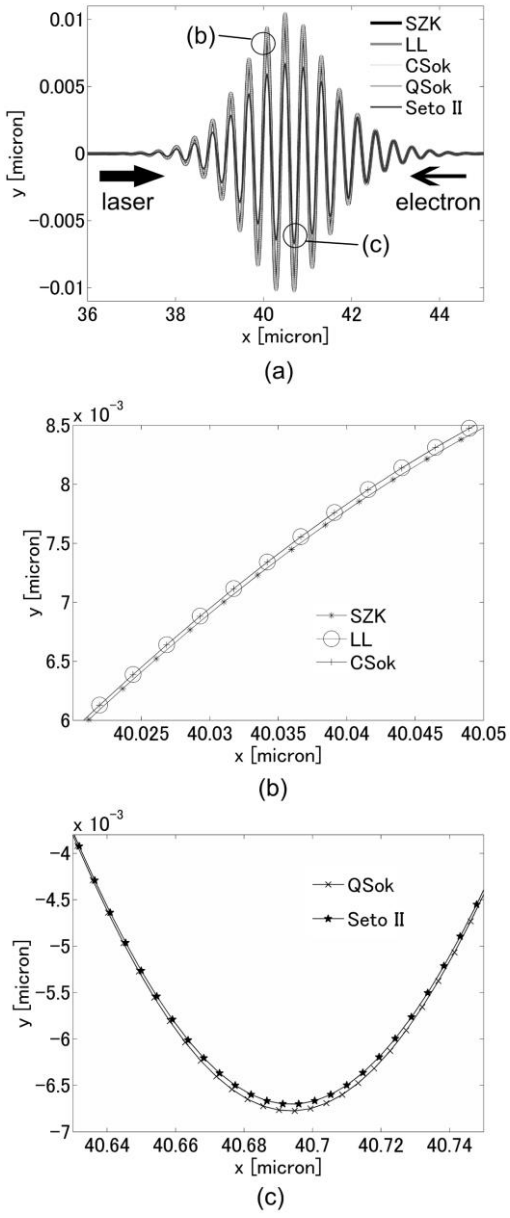

Figure 21 - Trajectory of a 600 MeV electron head-on colliding with the 1×10^{22} W/cm^2 laser pulse. (b) and (c) are the close-up figures of (a).

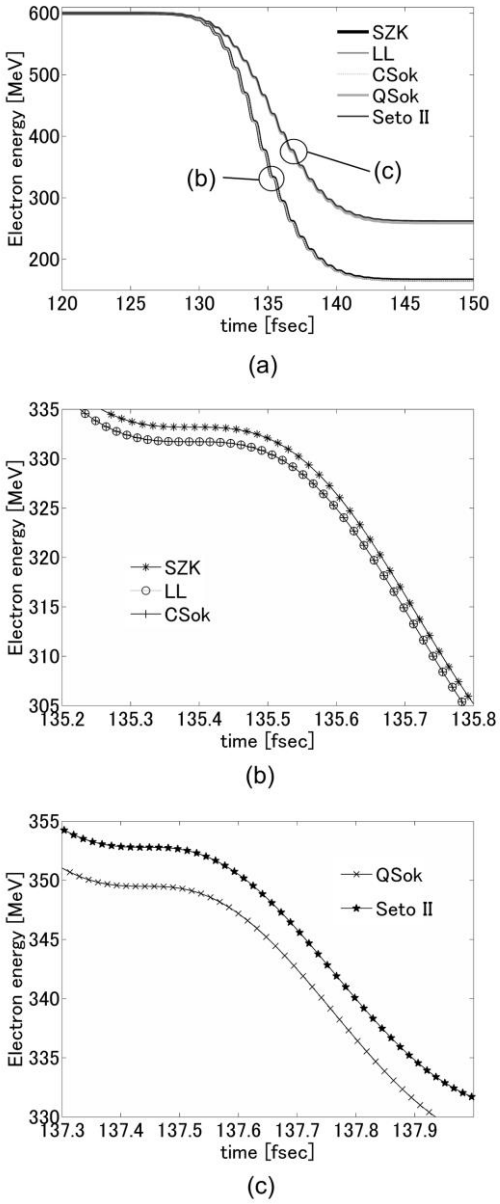

Figure 22 - Time evolution of electron energy. An electron of the initial energy of 600 MeV head-on collides with the 1×10^{22} W/cm^2 laser pulse. Due to radiation from an electron, we can find the energy drop of it and it represents the effect of RR. (b) and (c) are the close-up figures of (a).

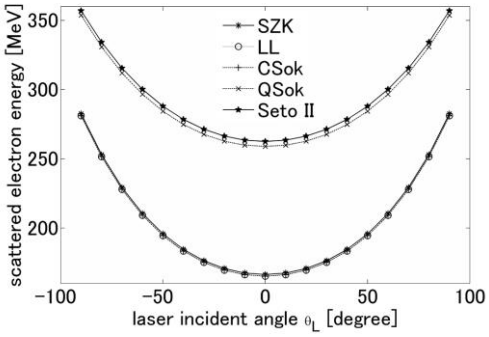

Figure 23 - Scattered electron energy vs. laser incident angle.

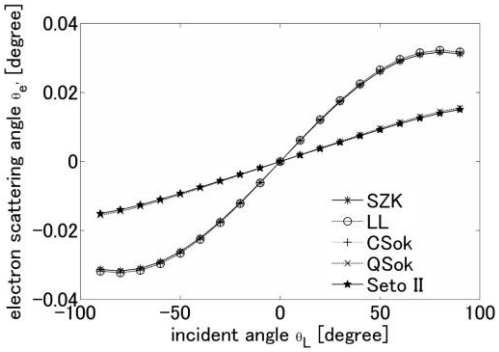

Figure 24 - Electron scattering angle vs. laser incident angle.

Figure 24 shows electron scattering angle estimated for various incident angles. The incident electron energy in the present case is large enough so that the electrons pass through the pulse laser without significant deflections.

Returning to the topic of the head-on collision case $\theta_L = 0$, Figure 25 shows angle distribution of photon energy per one incident beam electron. This calculation was carried out by using the angular resolution $d\theta = 2\pi/2^{11}$. Emitted photon energy is confined to small angles around the beam front direction, $\theta_\gamma = 0^\circ$ because parallel emission is dominant for high-energy electron (the spread angle of radiation is $d\theta_\gamma \sim (E_{\text{electron}} / m_0 c^2)^{-1}$, strong directivity). The emission angle distribution broadens up to $\theta_\gamma = O(10^\circ)$, which is wider than the angle distribution of scattered electron. This is because photon emission from oscillating electron directly contributes to the emission angle distribution. Thus, the emission spectrum measurement might provide an excellent indication for the model dependency of RR.

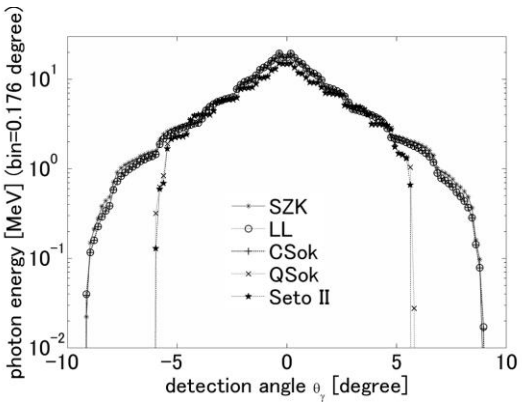

Figure 25 - Angular distributions of emitted photon energy in the case of the 1×10^{22} W/cm^2 laser and a 600 MeV electron. The calculation resolution of the detection angle is $d\theta=2\pi/2^{11}$.

3.2. The e^+e^- pair production in the Extremely Non-linear regime (RA5-Pair)

3.2.1. Introduction

Typical consequence of quantum electrodynamics (QED) is electron-positron pair production. Especially, pair production only by photons is attractive as a conversion process between matters and vacuum. There is a long history of theoretical work on this process from the beginning of QED. However experimental verification is not sufficient for these theories since it is difficult to realize the light source with enough energy to produce the electron-positron pairs.

There are several processes to realize the pair production in vacuum. One is the Breit-Wheeler process derived from perturbation theory of QED [49]. High-energy photons interact with each other and are converted into particle pairs. The threshold is determined by the total energy of the interacting two photons. The other is spontaneous pair production in a background electromagnetic field [50]. This process should be considered in the non-perturbative regime under the action of numerous photon interactions, which is not understood compared to the perturbative regime. The threshold is determined by the background field strength and is still far from the available laser intensities.

Fortunately, we can approach some part of the non-perturbative regime, i.e., strong-field QED, via a combined scheme: interaction between a strong laser field and high-energy photons [51]. Detailed cross sections have been obtained theoretically based on the semi-classical approach. The theory indicates that state-of-the-art intense lasers can potentially achieve the near threshold condition of pair

production. Possible pair production experiment in ELI-NP is considered to provide a proof of the strong-field QED.

In this proposal, we consider a simple experimental configuration similar to that of the previous experiment, SLAC E-144 [52]. The SLAC experiment is one of the few experimental examples on the pair production in laser fields. It is shown that SLAC and ELI-NP could approach different regimes of pair production, being complementary in the exploration of strong-field QED.

3.2.2. Physics Case

We describe several pictures of pair production in vacuum and their relevance to the present experiment in ELI-NP. Perturbation theory of QED derives pair production due to collision of two energetic photons. This is called Breit-Wheeler (BW) pair production [49]. Field energy associated with its strength also becomes an energy source of particle pair. Low frequency and strong field limit suggests spontaneous pair production from a constant but intense electromagnetic field [53, 50]. In the framework of QED, this process is regarded as a pair production from numerous low energy photons interacting simultaneously. Pair production in strong field is therefore not fully explored since non-perturbative treatment is required.

The spontaneous pair production is illustrated as a tunneling process in vacuum. Particles in the negative energy region can pass through the steep potential structure of background field by tunneling effect to reach the positive energy region. Probability of the tunneling process is estimated by using a typical electric field, i.e., Schwinger field $E_S \sim mc^2/e\lambda$, where λ denotes Compton wavelength. Resulting probability, P_S , is given as

$$P_S \propto \exp\left(-\pi \frac{E_S}{E}\right) \tag{3.2.1}$$

stands for the strength of background electric field [50]. The exponential dependency is a consequence of the tunneling effect.

Figure 26 shows typical diagrams of the pair production from high-energy photons. Panels (A) and (B) indicate single-photon and multi-photon BW processes [54], respectively. Threshold of single-photon BW process is determined by total photon energy in the center of mass system (CMS) of generated particle pair. The characteristic parameter, ξ is

$$\xi = \frac{s_{th}}{s}, \quad s_{th} = 4mc^2, \quad s = 4\omega\omega_L \tag{3.2.2}$$

where s_{th} and s are the minimum energy required for pair production and total photon energy in CMS, respectively, while ω and ω_L are photon energies. Head-on collision is assumed here. Threshold of single photon BW process is given by $\xi < 1$.

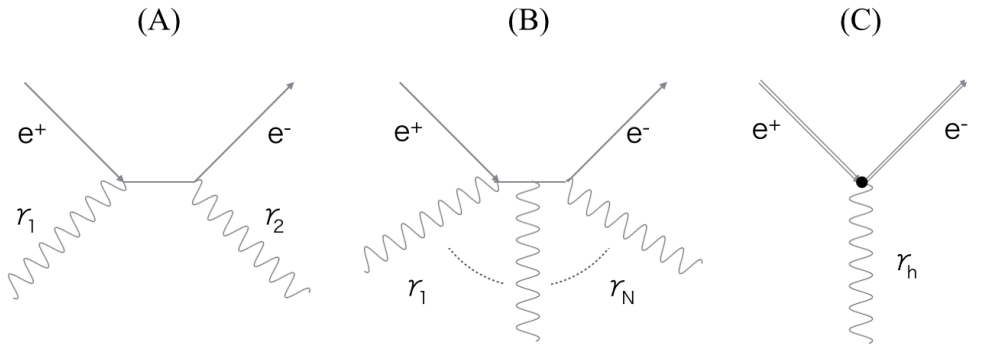

Figure 26 - Diagrams of typical pair production processes involving energetic photons. (A) single-photon BW process. Two photons γ_1 and γ_2 interact each other. (B) multi-photon BW process. N photons $\gamma_1 \ldots \gamma_2$ interact each other. (C) Pair production from energetic photon γ_h in strong field. Double lines indicate dressed particle.

For sub threshold case $\xi < 1$, particle pair can be generated only via multi-photon BH process. If additional photons come from a laser field, minimum number of interacting photon to produce one particle pair, $N_{\min}$, is estimated by

$$N_{\min} \sim \xi(1+\mathrm{a}^2), \quad a \equiv \frac{eE}{\omega_L mc} \tag{3.2.3}$$

where a is normalized vector potential of laser and ω_L is now laser frequency [52]. Required photon energy is quite large for single BW process in laser fields since laser frequency is small. For example, minimum photon energy is approximately 100 GeV for laser energy approximately 1 eV.

Figure 26 (C) represents pair production in strong field. Double lines stand for dressed electrons (or positrons) interacting with vast number of photons in external field [55]. Although the pair production is essentially non-perturbative, semi-classical approach can be applied for pair production triggered by an energetic photon in strong-field – stimulated pair production. Contribution of external field is exactly included in the dynamics of dressed particles [42, 48] and perturbative interaction is considered between the energetic photon and the dressed particles. Photon interaction in semi-classical regime is characterized by the quantum parameter χ,

$$\chi \equiv \frac{\lambda}{mc^2}\sqrt{-f_L \cdot f_L} = \frac{\lambda}{mc^2}\frac{e}{mc}\sqrt{-(F^{\mu\nu}p_\nu)^2} \tag{3.2.4}$$

where λ, $F^{\mu\nu}$ and p_ν denote Compton wavelength, field 4-tensor and 4-momentum of photon, respectively. Pair production cross section, $W_{pair}(\eta_+, \chi)$, is then

Table 6
Parameters of the available laser output

	electron energy [GeV]	electron number [$\times 10^9$]	laser intensity [W/cm^2]	photon energy [GeV]	E/Es (Spontaneous)	Nmin (multiphoton)	χ (strong field)	positron number
SLAC E-144	46.6	5	10^{18} (0.4)	< 30	< 10^{-5}	~5	< 0.20	0.2
ELI-NP (LINAC)	0.6	1	10^{22} (70)	< 0.35	< 10^{-3}	$10^{5\text{-}6}$	< 0.25	(~1)
ELI-NP (LWFA)	2.5	0.1	10^{22} (70)	< 1.5	< 10^{-3}	$10^{5\text{-}6}$	< 1.00	(> 10^4)

$$\frac{dW_{pair}(\eta_+,\chi)}{d\xi} = \frac{\alpha m^2 c^4}{\sqrt{3}\pi h\varepsilon_h}\left[\left(\frac{\eta_+}{\eta_-}+\frac{\eta_-}{\eta_+}\right)K_{2/3} + \int_\delta^\infty ds\, K_{1/3}(s)\right] \tag{3.2.5}$$

where α, h and ε_h are fine structure and Plank constants and photon energy, respectively. $\eta_+(\eta_-)$ denotes ratio of positron (electron) energies to photon energy, i.e., $\eta_- = \varepsilon_e/\varepsilon_h$ and $\eta_+ = 1-\eta_-$. δ is defined by $\delta = 2/3\times 1/\eta_-\eta_+\chi$ [48, 56]. Total cross section grows exponentially for χ larger than 1. Probability of pair production is roughly estimated as [57],

$$P \propto \exp\left(-\frac{8}{3}\frac{1}{\chi}\right) \tag{3.2.6}$$

This formulation invokes the tunneling effects as in the spontaneous pair production however the probability is determined by χ, not E/E_S.

We consider the relevance of above mentioned pair production processes to the experiments in ELI-NP [58] while comparing that in SLAC E-144 [52] experiment. Experimental parameters are summarized in Table 6 (left three columns: electron energy, number of electron per bunch and laser intensity (normalized potential). For ELI-NP, we consider two types of electron bunch. One is electron bunch from LINAC with energy of 600 MeV. The other is generated via laser wakefield acceleration. Considered electron energy is 2500 MeV [59]. Energy range of seed photon (the forth column) is roughly estimated by the energy spectrum of photon emitted from the incident electron bunch (experimental data for SLAC and simulation date for ELI-NP).

We estimate three typical parameters characterizing above-mentioned three pair production processes. Head-on collision between seed photon and pulse laser is assumed here. The first parameter E/E_S on spontaneous pair production (Eq.(3.2.1)) is quite small (less than 10^{-3}) even for ELI-NP as shown in the fifth column. Therefore, spontaneous pair production is still negligible. The second parameter $N_{\min}$ in the sixth column is required photon number in multi-photon BW process (Eq.(3.2.3)). $N_{\min}$ is quite different between ELI-NP (approximately 10^5-10^6) and SLAC (approximately 5). This estimation indicates that pair production could take place only in highly non-perturbative regime in ELI-NP while multi-photon process with a few photons is dominant in SLAC.

Despite this large difference of physical regime, the quantum parameter (Eq.(3.2.4)) in ELI-NP (600 MeV LINAC) has a value relatively close to that in SLAC, as shown in the seventh column. The quantum parameter is here estimated by $\chi \approx (E/E_s)(E_\gamma/mc^2)$, where E_γ is seed photon energy. Thus similar pair production rate is expected in strong field QED under the contribution of different number of laser photons.

Finally, generated positron number per electron bunch is given in the eighth column (observed positron number for SLAC and simulation results for ELI-NP). The simulation is based on the cross section described in Eq. (3.2.5). The expected positron number for 600 MeV electron beam is similar to the result of SLAC, as indicated in the quantum parameter. For 2.5 GeV case, the positron number increases significantly (greaterer than 10^4) compared to the other cases. This is a consequence of the exponential growth of pair production probability as in Eq. (3.2.6). Precise measurements of pair production rate and careful comparison with the result of SLAC experiment could provide a proof of the strong field QED.

3.2.3. Technical Proposal

The requirements and the experimental setup are identical to the ones for the experiments of radiation reaction, without any difference. For observing the e^+e^- pairs, removing the beryllium window as the γ -pairs converter (GPC).

3.2.4. Count Estimation

We estimate the pair production rate in the collision between electron beam and intense pulse laser. The estimation is based on a numerical simulation employing the cross sections of radiation and pair production. The cross sections are,

$$\frac{dW_{rad}(\xi_e,\chi)}{d\xi_e} = \frac{\alpha mc^2}{\sqrt{3}\pi\hbar\gamma}\left[\int_\delta^\infty dsK_{5/3}(s) + \left(1-\xi_e+\frac{1}{1-\xi_e}-2\right)K_{2/3}(\delta)\right]$$

$$\frac{dW_{pair}(\eta_+,\chi)}{d\xi} = \frac{\alpha m^2 c^4}{\sqrt{3}\pi\hbar\varepsilon_h}\left[\left(\frac{\eta_+}{\eta_-}+\frac{\eta_-}{\eta_+}\right)K_{2/3}(\delta)+\int_\delta^\infty dsK_{1/3}(s)\right] \tag{3.2.7}$$

where W_{rad} and W_{pair} are the cross section of radiation and pair production, respectively. χ, ξ_e and $\eta_+(\eta_-)$ are the quantum parameter, ratio of emitted photon energy to incident electron energy and ratio of positron (electron) energy to incident photon energy, respectively. δ is defined as $\delta = 2/3\times\xi_e/[(1-\xi_e)\chi]$ for radiation and $\delta = 2/3\times 1/(\eta_+\eta_-\chi)$ for pair production.

The experimental configuration is the same as that in RA5-RR. The primary process is again high-energy photon emission and its back reaction of electrons. The pair production is seeded by the emitted photons. That is, the pair production takes place as a two-step process,

$$\begin{aligned} &(1) \quad e^- + N\gamma_L \rightarrow e^- + \gamma_L \\ &(2) \quad \gamma_h + N\gamma_L \rightarrow e^+ + e^- \end{aligned} \tag{3.2.8}$$

where γ_h, γ_L and N denote high energy photon, laser photon and absorbed number of laser photon, respectively. In the present situation, particle pair is also generated via direct interaction between electron and laser field without high-energy real photon (trident pair production) [60-62]. Probability of this process is expected to be quite small compared to the two-step process. Thus this process is neglected in the simulation.

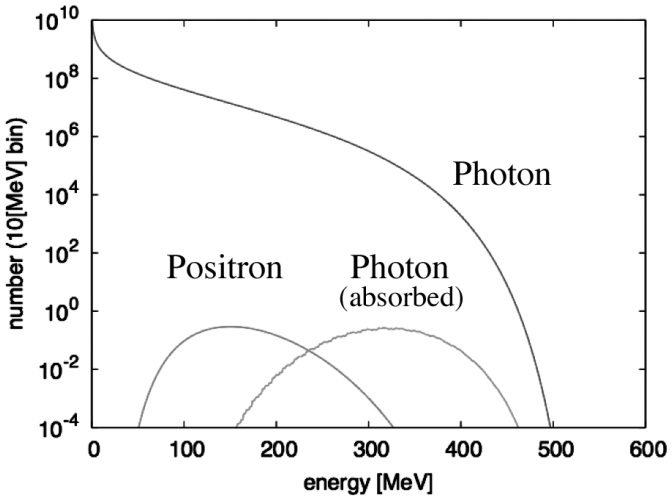

Figure 27 - Energy spectrum of emitted photon, absorbed photon and generated positron. Electron beam energy is 600 MeV. Energy bin size is 10 MeV.

Physical condition considered for the simulations are as explained in RA5-RR. Laser intensity, pulse duration, spot size are 10^{22} W/cm^2, 22 fs and 5 μm, respectively. Electron beam is obtained from accelerator and typical energy is 600 MeV. The other is obtained by using plasma wake field acceleration and energy is 2500 MeV.

Figure 27 shows the simulation results. The lines indicate energy spectrum of emitted photon, absorbed photon and generated positron. In this case, the quantum parameter is not so large (less than 0.25). Thus only small fractions of high-energy photons with energies in the range of 200-450 MeV are absorbed in the laser field, as shown in the purple line. Positron energy is roughly half of the absorbed photon energy, i.e., in the range of 100-300 MeV. Total number of positron per one electron beam (10^9 incident electrons) are approximately 1.

4. FUTURE EXTENSION: STAGE 2, 3 AND 4

Given the successful implementation of laser plasma acceleration, we can further plan the following upgrades or add new subjects as indicated in Figure 28.

"Stage 2" experiment is the realization of an all-optical table-top gamma-gamma collider at E4 (RA5-GG) to verify the QED-based elastic gamma-gamma scattering. This utilizes the same interaction chamber as that used for RA5-DM at E4. This proposal requires 210 MeV electrons by means of laser plasma acceleration (Research and Development topic).

"Stage 3" experiments essentially repeat the same measurements as those in the stage 1.5 with upgraded electron energies by means of laser plasma acceleration. Moreover, we aim at the production of linearly polarized 1 GeV gamma-ray source via the extremely nonlinear inverse Compton process with 5.0 GeV electrons for the next stage.

"Stage 4" experiment is measurement of vacuum birefringence (RA5-VBir) via the depolarization of linearly polarized energetic probe photons due to the effect of non-perturbative QED interactions in a focused high-intensity laser field.

Two ideas for further research were also proposed to ELI-NP and fit best the experimental setup in E7: i) Thomson backscattering in the extended lambda cubed regime for extension of the available gamma energy above 100 MeV range (D. Ursescu *et al.*) and ii) Compton backscattering using X-ray lasers for the extension of the available monochromatic gamma energy in the 400 MeV range (D. Ursescu *et al.*).

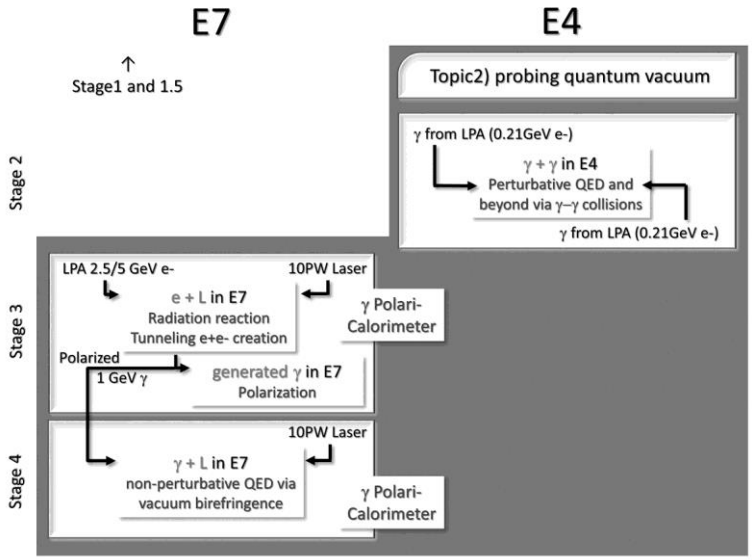

Figure 28 - Experimental setup of E7 – Stages 3 and 4.

***Acknowledgments*.** The authors wish to express their appreciation to Prof. Dietrich Habs for his great contribution to the entire ELI-NP project starting from early stage of proposal and for his continuous support. OT, LDA and KS were supported by the Project Extreme Light Infrastructure - Nuclear Physics (ELI-NP) - Phase I, a project co-financed by the Romanian Government and European Union through the European Regional Development Fund.

REFERENCES

1. P. Mohr *et al*., Phys. Lett. B **488**, 127 (2000).
2. H. Utsunomiya, P. Mohr, A. Zilges, M. Rayet, Nucl. Phys. A **777**, 459 (2006).
3. R. Capote *et al*., Nucl. Data Sheets **110**, 3107 (2009).
4. D.M. Brink, Ph.D. thesis, Oxford University, 1955.
5. D. Belic et al., Phys. Rev. Lett. **83**, 5242 (1999).
6. S. Goko et al., Phys. Rev. Lett. **96**, 192501 (2006).
7. E. Esarey, C. B. Schroeder, and W. P. Leemans, Rev. Mod. Phys. **81**, Phys. Rev. D **90**, 1229 (2009).
8. R. D. Peccei and H. R. Quinn, Phys. Rev. Lett. **38**, 1440 (1977); S. Weinberg, Phys. Rev. Lett. **40**, 223 (1978); F. Wilczek, Phys. Rev. Lett. **40**, 271 (1978).

9. Y. Fujii and K. Maeda, *The Scalar-Tensor Theory of Gravitation* Cambridge Univ. Press (2003); Mark P. Hertzberg, Max Tegmark, and Frank Wilczek, Phys. Rev. D **78**, 083507 (2008); Olivier Wantz and E. P. S. Shellard, Phys. Rev. D **82**, 123508 (2010).
10. K. Homma, D. Habs, T. Tajima, Appl. Phys. B **106**:229-240 (2012), (DOI: 10.1007/s00340-011-4567-3), arXiv:1103.1748 [hep-ph].
11. T. Tajima and K. Homma, Int. J. Mod. Phys. A vol. **27**, No. 25, 1230027 (2012).
12. Kensuke Homma, Takashi Hasebe, KazukiKume, Prog. Theor. Exp. Phys. **2014**, 083C01 (2014).
13. K. Ehret et al. (ALPS Collab.), Phys. Lett. B **689**, 149 (2010).
14. E. G. Adelberger et al., Phys. Rev. Lett. **98**, 131104 (2007); D. J. Kapner et al., Phys. Rev. Lett. **98**, 021101 (2007).
15. J. Chiaverini et al., Phys. Rev. Lett. **90**, 151101 (2003).
16. S. J. Smullin et al., Phys. Rev. **D 72**, 122001 (2005) [Erratum-ibid. D **72**, 129901 (2005)].
17. S. K. Lamoreaux, Phys. Rev. Lett. **78**, 5 (1997) [Erratum-ibid. **81**:5475 (1998)].
18. See the parametrization, for example, in the section AXIONS AND OTHER SIMILAR PARTICLES in J. Beringer et al. (Particle Data Group), Phys. Rev. D **86**, 010001 (2012). And also see S. L. Cheng, C. Q. Geng, and W. T. Ni, Phys. Rev. D **52**, 3132 (1995) on the possible range of the ratio on the electromagnetic to color anomaly factors of the axial current associated with the axion, E/N.
19. J. E. Kim, Phys. Rev. Lett. **43**, 103 (1979); M. A. Shifman, A. I. Vainshtein and V. I. Zakharov, Nucl. Phys. B **166**, 493 (1980).
20. K. Seto, J. Koga, S. Zhangm Review of Laser Engineering, **42**, 2, 174 (2014).
21. G.A. Mourou, N.J. Fisch, V.M. Malkin, Z.Toroker, E.A. Khazanov, A.M. Sergeev, T.Tajima and B.LeGarrec, Opt. Comm. 720 **285** (2012).
22. D. Habs, T. Tajima and V. Zamfir, Nuclear Physics News **21**, 23 (2011).
23. J. Koga, Phys. Rev. E **70** 046502 (2004).
24. A. Zhidkov, J. Koga, A. Sasaki and M. Uesaka, Phys. Rev. Lett. **88** 18 (2001).
25. H. A. Lorentz, *The Theory of Electrons and Its Applications to the Phenomena of Light and Radiant Heat, A Course of Lectures Delivered in Columbia Univ., New York, in March and April 1906*, 2nd edition (Teubner, Leipzig, 1916).
26. M. Abraham, *Theorie der Elektrizität: ElektromagnetischeTheorie der Strahlung*, (Teubner, Leipzig, 1905).
27. P. A. M. Dirac, Proc. Roy Soc. A **167**, 148 (1938).
28. J. Larmor, Phil. Trans. Roy. Soc. London A, **190**, 205 (1897).
29. J. D. Jackson, *Classical Electro-dynamics, 3rd Ed.* (John Wiley & Sons, New York, 1998).
30. W. K. H. Panofski and M. Phillips, *Classical Electricity and Magnetism, 1st edition* (Addison - Wesley Publishing Inc., Cambridge, 1961).
31. Shinichiro Tomonaga, Prog. Theor. Phys. **1**, 27 (1946).
32. J. Schwinger, Phys. Rev. **74**, 1439 (1948).
33. R. Feynman, Phys. Rev. **76**, 769 (1949).
34. A. Liénard, L'Éclaiarge Électrique **16**, 5-14, 53-59, 106-112 (1898).
35. E. Wiechert, Annalen der Physik **309**, 667 (1901).
36. G. Farmelo, *THE STRANGEST MAN The hidden Life of Paul Dirac, Quantum Genius*, Ch. 21, (Faber and Faber, London, 2009).
37. Proc. Roy Soc. A **194**, 543 (1948).
38. G. W. Ford and R. F. O'Connell, Phys. Lett. A **174**, 182-184 (1993).
39. L. D. Landau and E. M. Lifshitz, *The Classical theory of fields* (Pergamon, New York, 1994).
40. F. A. Rohrlich, Phys. Lett. A **283**, 276 (2001).
41. I. V. Sokolov, J. Exp. Theo. Phys. **109**, No.2 (2009).
42. A. I. Nikishov, V. I. Ritus, Sov. Phys. JETP **19**, 529(1964).
43. A. A. Sokolov and I. M. Ternov, "Radiation from Relativistic Electrons", American Institute of Physics (translation series, 1986).
44. I. V. Sokolov, N. M. Naumova and J. A. Nees, Phys. Plasma **18**, 093109 (2011).

45. K. Seto, S. Zhang, J. Koga, H. Nagatomo, M. Nakai and K. Mima, Prog. Theor. Exp. Phys **2014**, 043A01 (2014), also arXiv:1310.6646v3, (2013).
46. K. Seto, Prog. Theor. Exp. Phys **2015**, 023A01 (2015), also arXiv: 1405.7346v4 (2014).
47. K. Seto, Prog. Theor. Exp. Phys **2015**, 103A01 (2015), arXiv: 1502. 05319v4.
48. D. M. Volkov, Z. Phys. **94**, 250 (1935).
49. G. Breit and J. A. Wheeler, Phys. Rev. **46**, 1087 (1934).
50. J. S. Schwinger, Phys. Rev. **82**, 664 (1951).
51. R. Schutzhold et al., Phys. Rev. Lett. **101**, 130404 (2008).
52. C. Bamber, S. J. Boege, T. Koffas et al, Phys. Rev. D **60**, 092004 (1999)。
53. J. Sauter, Phys. Rev. **82**, p. 664 (1951).
54. H. R. Reiss, J. Math. Phys. **3**, 59 (1962).
55. W.H. Furry, Phys.Rev, **81**, 115, (1951).
56. V. B. Berestetskii, E. M. Lifshits, and L. P. Pitaevskii, Quantum Electrodynamics (Pergamon, New York, 1982).
57. N.B. Narozhnyi, Sov. Phys. JETP **27**, 360 (1968).
58. L. Ionela and D. Ursescu, Laser and Particle Beams **32**, 89 (2014).
59. N. Nakajima, Eur. Phys. J. Special Topics **223**, 999–1016 (2014).
60. A. Ilderton, Phys. Rev. Lett. **106**, 020404 (2011).
61. H. Hu, Carsten Müller and C. H. Keitel, Phys. Rev. Lett. **105**, 080401 (2010).
62. B. King and C. H. Keitel, New J. Phys. **14**, 103002 (2012).